# The labile interactions of cyclic electron flow effector proteins

Felix Buchert, Marion Hamon, Philipp Gäbelein, Martin Scholz, Michael Hippler, Francis-André Wollman

# The labile interactions of cyclic electron flow effector proteins

Received for publication, June 14, 2018, and in revised form, September 5, 2018 Published, Papers in Press, September 18, 2018, DOI 10.1074/jbc.RA118.004475

**Felix Buchert[‡§], Marion Hamon[¶], Philipp Gäbelein[§], Martin Scholz[§], Michael Hippler[§], and Francis-André Wollman[‡1]**

*From the [‡]Institut de Biologie Physico-Chimique, UMR7141 CNRS-Sorbonne-Université, 13 Rue P et M Curie, 75005 Paris, France, the [§]Institute of Plant Biology and Biotechnology, University of Münster, Schlossplatz 8, 48143 Münster, Germany, and the [¶]Institut de Biologie Physico-Chimique, UMR8226/FRC550 CNRS-Sorbonne-Université, 13 Rue P et M Curie, 75005 Paris, France*

Edited by Joseph M. Jez

**The supramolecular organization of membrane proteins (MPs) is sensitive to environmental changes in photosynthetic organisms. Isolation of MP supercomplexes from the green algae *Chlamydomonas reinhardtii*, which are believed to contribute to cyclic electron flow (CEF) between the cytochrome $b_6f$ complex (Cyt-$b_6f$) and photosystem I (PSI), proved difficult. We were unable to isolate a supercomplex containing both Cyt-$b_6f$ and PSI because in our hands, most of Cyt-$b_6f$ did not comigrate in sucrose density gradients, even upon using chemical cross-linkers or amphipol substitution of detergents. Assisted by independent affinity purification and MS approaches, we utilized disintegrating MP assemblies and demonstrated that the algae-specific CEF effector proteins PETO and ANR1 are *bona fide* Cyt-$b_6f$ interactors, with ANR1 requiring the presence of an additional, presently unknown, protein. We narrowed down the Cyt-$b_6f$ interface, where PETO is loosely attached to cytochrome *f* and to a stromal region of subunit IV, which also contains phosphorylation sites for the STT7 kinase.**

Photosynthesis converts solar energy into electrochemical energy, which eventually enables $CO_2$ fixation by the Calvin–Benson–Bassham cycle enzymes (1). To ensure assimilation of fixed carbon, ATP and NADPH serve as energy currencies that are produced during photosynthetic electron transfer. Two photosynthesis modes exist in higher plants and green algae (2), termed linear electron flow (LEF)[2] and cyclic electron flow (CEF). Their contribution to total electron transfer depends on environmental cues. Whereas LEF theoretically provides ATP and NADPH at a ratio of 2.6:2, enzymatic $CO_2$ fixation requires a ratio of 3:2. To overcome this metabolic restraint, CEF balances out the increased demand for ATP. Indeed, CEF allows only ATP synthesis because electrons produced by photooxidation of the primary donor of photosystem I (PSI) re-enter the electron transport chain either at the plastoquinone (PQ) pool or at the stromal side of the Cyt-$b_6f$. Thus, depending on the site of re-injection of reducing equivalents into the membrane, several CEF pathways may exist. One involves PQ reductases from the chlororespiration pathway (3), a type-1 NADH dehydrogenase-like complex (NDH) in higher plants (4), and a type-2 NAD(P)H dehydrogenase in the algal model organism *Chlamydomonas reinhardtii* (5), hereafter referred to as *Chlamydomonas*. However, with less than 3 e $s^{-1}$ $PSI^{-1}$ the kinetics of electron flow through this pathway is too sluggish (6) (reviewed by Nawrocki *et al.* (7)) to match the rates of electron transfer though CEF, which are well above 10 e $s^{-1}$ $PSI^{-1}$, transiently reaching up to 130 e $s^{-1}$ $PSI^{-1}$ in plant chloroplasts (8). Another pathway, the PGR-dependent CEF, involves the proteins proton gradient regulation 5 (PGR5) and *pgr5*-like photosynthetic phenotype 1 (PGRL1), which has been proposed to have a ferredoxin-PQ oxidoreductase activity (9–11). However, a PGRL1-defective mutant of *Chlamydomonas* is still capable of high rates of CEF (12). Thus, a third route, still awaiting further documentation, involves direct electron donation through the ferredoxin-$NADP^+$ oxidoreductase (FNR) bound to Cyt-$b_6f$, making use of heme $c_i$ next to the PQ binding site $Q_i$ (8, 13–15). Whatever the route, CEF competes for electrons with other, oxygen-consuming reactions involving flavodiiron proteins (16, 17) or the Mehler reaction. When oxygen is lacking in the algae, CEF is stimulated upon establishing a strongly reduced PQ pool in response to a lowered intracellular ATP/NADPH ratio (18). The reduced PQ pool also activates the STT7 kinase, which facilitates migration of light-harvesting complex II (LHCII) and Cyt-$b_6f$ to the unstacked regions of thylakoid membranes (19, 20). Recently, profound CEF-related rearrangements were described in *Chlamydomonas*, resulting in the formation of a CEF supercomplex (21). The purported supercomplex was reported to consist of PSI and Cyt-$b_6f$, as well as of proteins from the light-harvesting complex I (LHCI) family and mobile LHCII. PGRL1 and FNR were also detected

This work was supported by CNRS and the "Initiative d' Excellence" Program from the French state grant "DYNAMO", ANR-11-LABX-0011-01. This work was also supported by Deutsche Forschungsgemeinschaft (DFG) Grant HI 739/13-1 (to M. H.). The authors declare that they have no conflicts of interest with the contents of this article.
This article contains Tables S1 and S2 and Figs. S1–S9.

[1] To whom correspondence should be addressed. Tel. 33-1-5841-5012; Fax: 33-1-5841-5022; E-mail: Wollman@ibpc.fr.

[2] The abbreviations used are: LEF, linear electron flow; PQ, plastoquinone; SDG, sucrose density gradient; TDM, *n*-tridecyl β-maltoside; αDM, *n*-dodecyl α-maltoside; PMal-C8, poly(maleic anhydride-alt-1-decene) substituted with 3-(dimethylamino)propylamine; PSI, photosystem I; PSII, photosystem II; LHC, light-harvesting complex; FCCP, carbonyl cyanide-4-(trifluoromethoxy)phenylhydrazone; DSP, dithiobis(succinimidyl propionate); DSS, disuccinimidyl suberate; Cyt-$b_6f$, cytochrome $b_6f$ complex; su-IV, subunit IV of the Cyt-$b_6f$ encoded by *petD*; Cyt-*f*, cytochrome *f* of the Cyt-$b_6f$ encoded by *petA*; Fd, ferredoxin; FNR, Fd-$NADP^+$ oxidoreductase; Chl, chlorophyll; MP, membrane protein(s); CEF, cyclic electron flow; NDH, NADH dehydrogenase-like complex; 2D, two-dimensional; TAP, Tris acetate phosphate; Tricine, *N*-[2-hydroxy-1,1-bis(hydroxymethyl)ethyl]glycine.

within this supercomplex. When illuminated, an *in vitro*–purified CEF supercomplex accepted electrons from NADPH via ferredoxin (Fd). Furthermore, the PSI primary electron donor $P700^+$ was photoreduced by added plastocyanin. This CEF supercomplex preparation was devoid of PGR5. Based on various reports, other auxiliary proteins are believed to be part of the CEF supercomplex in *Chlamydomonas* as well. Among these CEF effectors are the algal proteins PETO (18, 21) and anaerobic response 1 (ANR1) (22). Although PETO (23) and ANR1 (22) facilitate CEF, their exact function and stoichiometry with respect to other CEF components remain elusive. ANR1 expression is stimulated when *Chlamydomonas* is kept in anoxic conditions (24). In a recent study, a decreased ANR1 accumulation was observed in PETO-overexpressing lines (23). Therein, it was suggested that PETO is the main interactor of ANR1. PETO contains a lumenal N terminus that is separated from a stromal C terminus by a single transmembrane helix (25). The phosphoprotein was originally referred to as "subunit V" of the Cyt-$b_6f$ complex (26). PETO, largely depleted in Cyt-$b_6f$ mutant strains, was later considered as a loosely attached subunit that co-purifies with the Cyt-$b_6f$ in the early stages of a multistep protocol (25). The two algal CEF effectors were indirectly intertwined with the Cyt-$b_6f$, like FNR in higher plants (13, 14). However, they are not structurally characterized (27); nor were they shown to be genuine Cyt-$b_6f$ interactors. Still, ANR1, PETO, FNR, and PGRL1 frequently formed high molecular weight complexes, which has been suggested to result from the ability of these relatively small CEF effector proteins to adopt an oligomeric configuration (23).

In previous studies, the CEF supercomplex was extracted from thylakoid samples that were solubilized with alkyl maltosides, specifically $\alpha$- and $\beta$-glycosides of *n*-dodecyl maltoside (22, 28) as well as *n*-tridecyl $\beta$-maltoside (18, 21, 23). The solubilized proteins were separated according to their apparent molecular weight via rate-zonal centrifugation using sucrose density gradients (SDGs). However, the loose attachment of CEF effectors with the CEF core (18, 25, 27, 29) and the partial disassembly of the CEF supercomplex at elevated ionic strength (21) have hampered its further molecular and functional characterization over the last few years. Indeed, the preparation procedures after the solubilization step span a 16–24-h time period during which original interactions within the extracted CEF supercomplex might be compromised. The preservation of the genuine components of a transmembrane supercomplex is thus a major challenge when characterizing membrane proteins (MPs) in a detergent environment (reviewed by Seddon *et al.* (30)). In that respect, replacing detergents with amphipol surfactants holds promises to stabilize solubilized MPs in aqueous solution (reviewed by Zoonens and Popot (31)).

In this work, we carefully revisited the experimental conditions that were previously reported to produce solubilized CEF supercomplexes in heavy SDG fractions. Despite our efforts, which used a series of different approaches to stabilize critical protein interactions and are outlined in the first two sections under "Results," we were not able to isolate a CEF supercomplex at a reproducibly high yield. Therein, we address limitations of the SDG approach by showing that the chlorophyll (Chl) content of high-sucrose density fractions is highly sensitive to sample handling during the solubilization step. Green bands in heavy SDG fractions, containing PSI, LHCI, LHCII, and other CEF effectors, were obtained independently of the presence of Cyt-$b_6f$, which necessitates caution in the identification of a CEF green band. We also explored how the detergent concentration within SDG, which varied in published protocols, alters migration of CEF effectors, and we discuss potential caveats for the interpretation of SDG experiments. Nevertheless, our experimental conditions, although destabilizing the most labile protein interactions, enabled us in the later sections to obtain new insights into CEF-related protein interactions. Assisted by cross-link experiments and MS, we utilized the lability of the system to characterize the interface of the algal CEF effector PETO with Cyt-$b_6f$ at a molecular level, thus finally proving that PETO is a subunit of the algal Cyt-$b_6f$. We also trapped solubilized MPs with amphipols, concluding that heavy assemblies of CEF effectors in SDG were likely aggregates resulting from detergent-induced destabilization during rate-zonal centrifugation. The amphipol approach in combination with cross-link experiments argues for the algal CEF effector ANR1 to be cross-linked to Cyt-$b_6f$ via a yet unknown protein(s). The potential role of the loosely bound algal Cyt-$b_6f$ subunits is discussed in the context of CEF.

## Results

### *The high-density fractions in n-tridecyl β-maltoside (TDM)-containing SDG lack Cyt-$b_6f$*

Here, we will tie in with the protocol by Takahashi *et al.* (18), which we used previously to assign heavy, Chl-containing SDG fractions as CEF supercomplexes. Our protocol was developed, like other variants (22, 28, 32), to build on the original findings by Iwai *et al.* (21), which we will return to in the next section as an attempt to improve the poor Cyt-$b_6f$ retention in heavy SDG fractions in our hands.

Rate-zonal centrifugation is routinely used to isolate solubilized MPs in different SDG fractions. This method has the advantage over native PAGE of allowing subsequent *in vitro* analysis of a CEF supercomplex. For its characterization in *Chlamydomonas*, various procedures were described that use alkyl maltosides as detergents (18, 21, 22). Four crucial steps differed between these studies: first, the heterotrophically grown algae were exposed differently to state 2–inducing conditions by inhibiting mitochondrial respiration, thus depleting ATP and increasing reducing equivalents in the chloroplast due to the Pasteur effect (33). This was done either in the presence of the membrane uncoupler FCCP (21) or by removing oxygen from the medium (18, 22). Then cells were disrupted either with a nebulizer (21, 22) or a French press (18), followed by thylakoid membrane isolation using a modified protocol published by Chua and Bennoun (34). Another main difference for thylakoid isolation was the buffer system, which was either MES at pH 6.5 (21) or HEPES at pH 7.5 (18, 22). Finally, the use of the detergent for solubilization and SDG centrifugation differed, whereas the solubilization step was at ~1% (w/v) detergent per mg of Chl. Both $\alpha$- and $\beta$-glycosides of dodecyl maltoside (22, 28) have been used, with *n*-dodecyl $\alpha$-maltoside ($\alpha$DM) producing milder conditions. An even milder detergent,

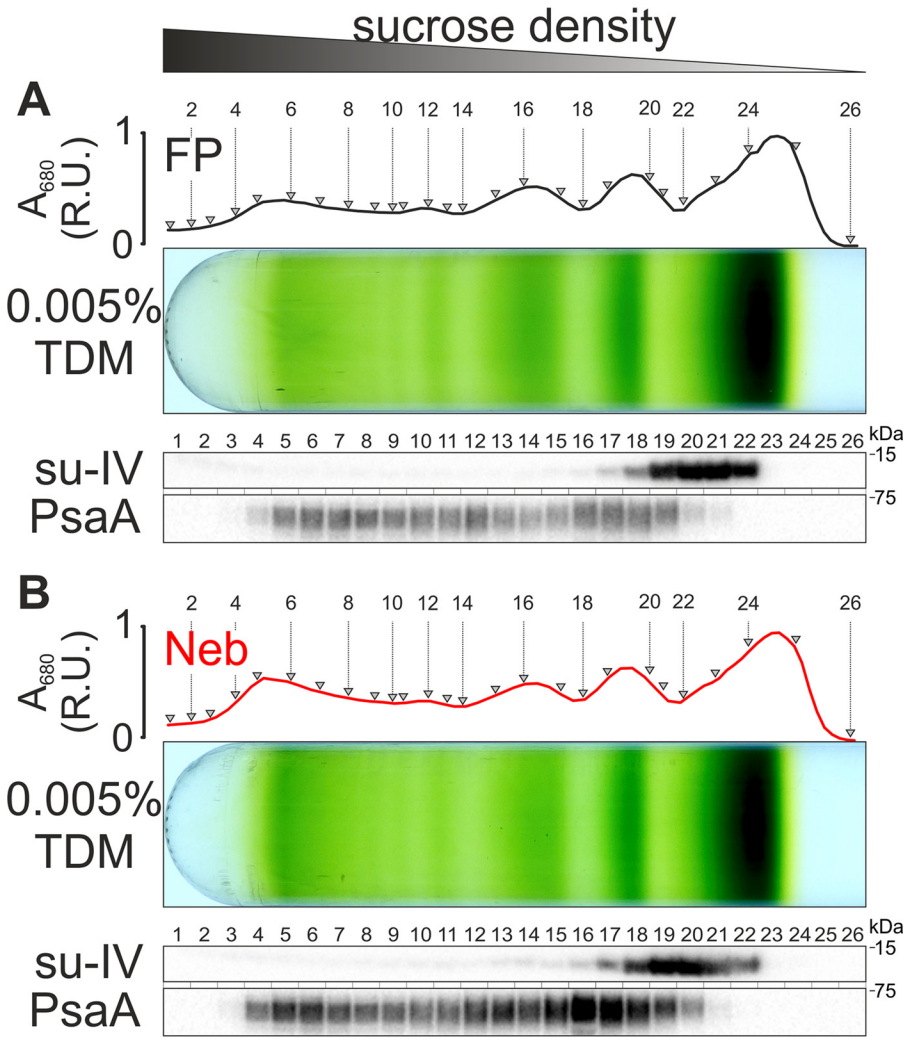


**Figure 1. Despite different cell disruption methods, a poor comigration of PSI and Cyt-$b_6f$ was observed upon SDG ultracentrifugation.** As described under "Experimental procedures," the harvested cc-124 WT cells were subjected to state 2–inducing anoxic conditions, and cell disruption was carried out with a French press (*FP*) (*A*) or by using the gentler nebulizer method (*Neb*) (*B*). Thylakoids were isolated in a HEPES buffer as described previously (18). Independently of the disruption method, su-IV of the Cyt-$b_6f$ was found mainly in fractions 16–22 in the SDG. The smearing PSI, probed via PsaA, peaked in fractions 15–19 with minor peaks in fractions 12 and 13 and at high-sucrose density fractions 5–8. *R.U.*, relative units of normalized Chl absorbance at 680 nm.

TDM, has been introduced (18, 21) and was used in this study. The sucrose concentration in the discontinuous gradient ranged from 1.3 to 0.1 M, and the corresponding detergent concentration (w/v) in the SDG was 0.05% (21, 22) and 0.005% (18), respectively.

The protocol from Takahashi *et al.* (18) uses French press cell disruption and frozen/thawed thylakoids before the solubilization step. The latter treatment proved not necessary (Fig. S1) and was thus omitted in our experiments. As compared with the use of a nebulizer, breaking the cells more effectively via French press (see "Experimental procedures") could disrupt weak protein interactions. We show in Fig. 1 that the two cell disruption modes produced the same set of major green bands. The Chl-binding LHCs were probed in Fig. S2. A set of overlapping bands culminated in a diffuse high-density green band in fractions 4–7, which was greener when using the nebulizer. Independently of the disruption method, the heavy PSI-containing fractions were greener if the reaction tubes were inverted every 5 min during the solubilization step (Fig. 1) instead of flicked (Fig. S3). Nonetheless, the distribution of the other core component of the CEF supercomplex, the Cyt-$b_6f$, was confined between the PSI and the PSII band in the upper part of the gradient (fractions 16–22, Fig. 1). We saw, however, different Cyt-$b_6f$ distributions in the SDG that resulted even in faint signals at the very bottom fraction. Clearly, the Cyt-$b_6f$/PSI signals were not well-aligned in the heavy SDG fractions, and thus, we were unable to produce a CEF supercomplex in these experimental conditions. In agreement with other reports (18, 23), the auxiliary CEF effectors were detected in the very bottom fractions of the SDG as well. In particular, the green high-sucrose density fractions 3–7 contained PSI, LHC from both photosystems, and the auxiliary CEF proteins PETO, ANR1, and PGRL1 (Fig. 2*A*). Again, neither cytochrome *f* (Cyt-*f*) nor subunit IV (su-IV) were detected in the lower SDG region. Despite the absence of the Cyt-$b_6f$, a ΔCyt-*f* mutant produced a very similar protein distribution (Fig. 2*B*). However, PETO was hardly detectable in solubilized ΔCyt-*f* thylakoid membranes, consistent with the report that PETO accumulation depends on that of Cyt-$b_6f$ (23, 25, 26). Interestingly, the same holds true for ANR1. It should be noted that, due to the

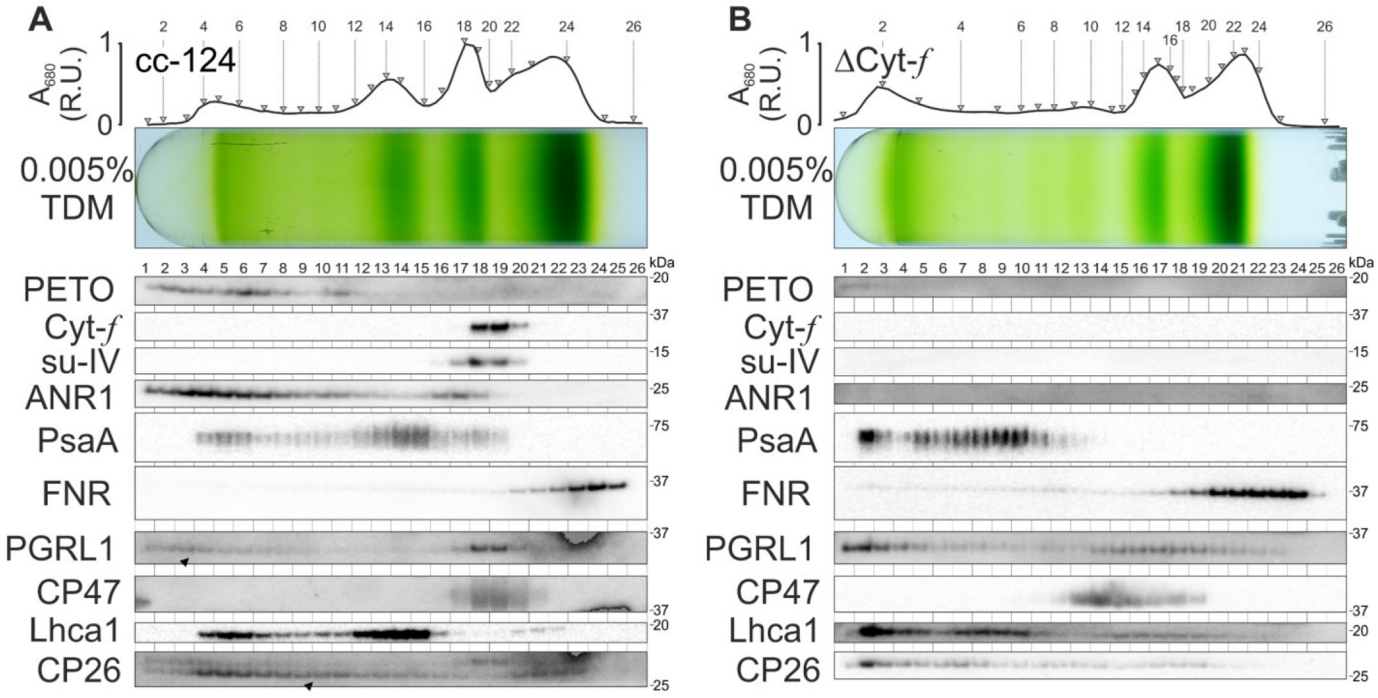


**Figure 2. CEF supercomplex components migrate into high-sucrose density fractions independently of the Cyt-$b_6f$.** The conditions were as in Fig. 1*A*. *A*, the *top three green bands* of solubilized cc-124 WT thylakoids migrated similarly as in Fig. 1*A*. Due to disperse pigmentation, the *fourth green band* in fraction 10 was hardly distinguishable, and at the *bottom* of the gradient (fractions 4–7) a *fifth green band* appeared, which contained CEF supercomplex components (21) except for Cyt-$b_6f$ and FNR. The latter was found in low-sucrose density fractions 20–25. PETO, ANR1, and PGRL1 migrated up to the bottom of the SDG. PGRL1 showed a second peak cofractionating with PSII and Cyt-$b_6f$. *B*, the *green high-sucrose density band* was produced in a mutant devoid of Cyt-$b_6f$, harboring a mutation in *petA* (66). The strain showed protein distribution similar to that of the WT, whereas PGRL1 showed broader signals in the upper half of the SDG. ANR1 and PETO were strongly underrepresented in solubilized thylakoids. *R.U.*, relative units of normalized Chl absorbance at 680 nm.

absence of Cyt-$b_6f$, the ΔCyt-*f* mutant was locked in state 1 despite the pretreatment (26, 35). Nevertheless, state transitions are not a prerequisite for CEF and for the production of Chl-containing heavy SDG fractions (18).

In the next section, we tested whether the original protocol by Iwai *et al.* (21) was more suitable to retain Cyt-$b_6f$ in high-sucrose density regions together with PSI.

### *The original isolation protocol, in combination with dithiobis(succinimidyl propionate) (DSP) cross-link treatment, still produced poor Cyt-$b_6f$ retention in the high-sucrose density fractions*

To use experimental conditions closer to the initial report on a CEF supercomplex isolation in *Chlamydomonas* (21), we inhibited mitochondrial respiration with FCCP before cell disruption via French press, and a MES buffer was used at pH 6.5 for thylakoid membrane isolation. In accordance with the studies by Iwai *et al.* (21), the protocol yielded four distinct green bands. However, in our hands, the Cyt-$b_6f$ content in the lower green band remained very limited (fractions 7–10 in Fig. 3*A*).

At variance with the experimental conditions used in Figs. 1 and 2, Fig. 3 results from a 10-fold higher TDM concentration in SDG, hereafter referred to as high-TDM SDG, which contained 0.05% (w/v) TDM. In contrast, the SDG from Figs. 1 and 2 contained 0.005% (w/v) TDM, referred to as low-TDM SDG. When following the procedure used by Takahashi *et al.* (18) but using high-TDM SDG (Fig. 3*B*), the ultracentrifugation of solubilized state 2 thylakoids produced three green bands and a pale band (fractions 7–9) below the PSI band. The heaviest SDG fractions were devoid of PSI and colorless, unlike in the original Takahashi *et al.* (18) conditions (Fig. 2*A*). The FNR distribution was also markedly changed. In low-TDM SDG (Fig. 2*A*), FNR migrated in low-density fractions, whereas in high-TDM SDG (Fig. 3*B*), FNR mainly peaked with PSI in fractions 9–14 (both panels are assembled in Fig. S4 for comparison). However, FNR was also present in upper fractions, such as 16–21, where Cyt-$b_6f$ was detected with a slight offset to the PSII core marker CP47. Given their respective molecular mass, SDG comigration of the monomeric PSII core complex (36) with the ~220-kDa Cyt-$b_6f$ homodimer is expected (27, 37).

Here again, the experimental conditions used above were not suitable to obtain significant comigration of PSI and Cyt-$b_6f$ as core elements of a putative CEF supercomplex. We then combined the conditions of Iwai *et al.* (21) with a low-TDM SDG at 0.005% but did not get a major enrichment in PSI/Cyt-$b_6f$ comigration (Fig. S5).

Because we found no conditions to recover a significant proportion of Cyt-$b_6f$ in high-sucrose density fractions, we attempted to overcome a putative dissociation of the purported CEF supercomplex by using the reversible cross-linker DSP. This homobifunctional cross-linker is thiol-cleavable and targets Lys within a 1.2-nm distance. Before their solubilization, isolated thylakoids were incubated with DSP. This pretreatment did not modify the distribution of green bands in the Iwai *et al.* (21) conditions (Fig. 3*C*) when compared with untreated samples in Fig. 3*A*. However, after cleaving DSP cross-links in selected SDG fractions and investigating the CEF supercom-

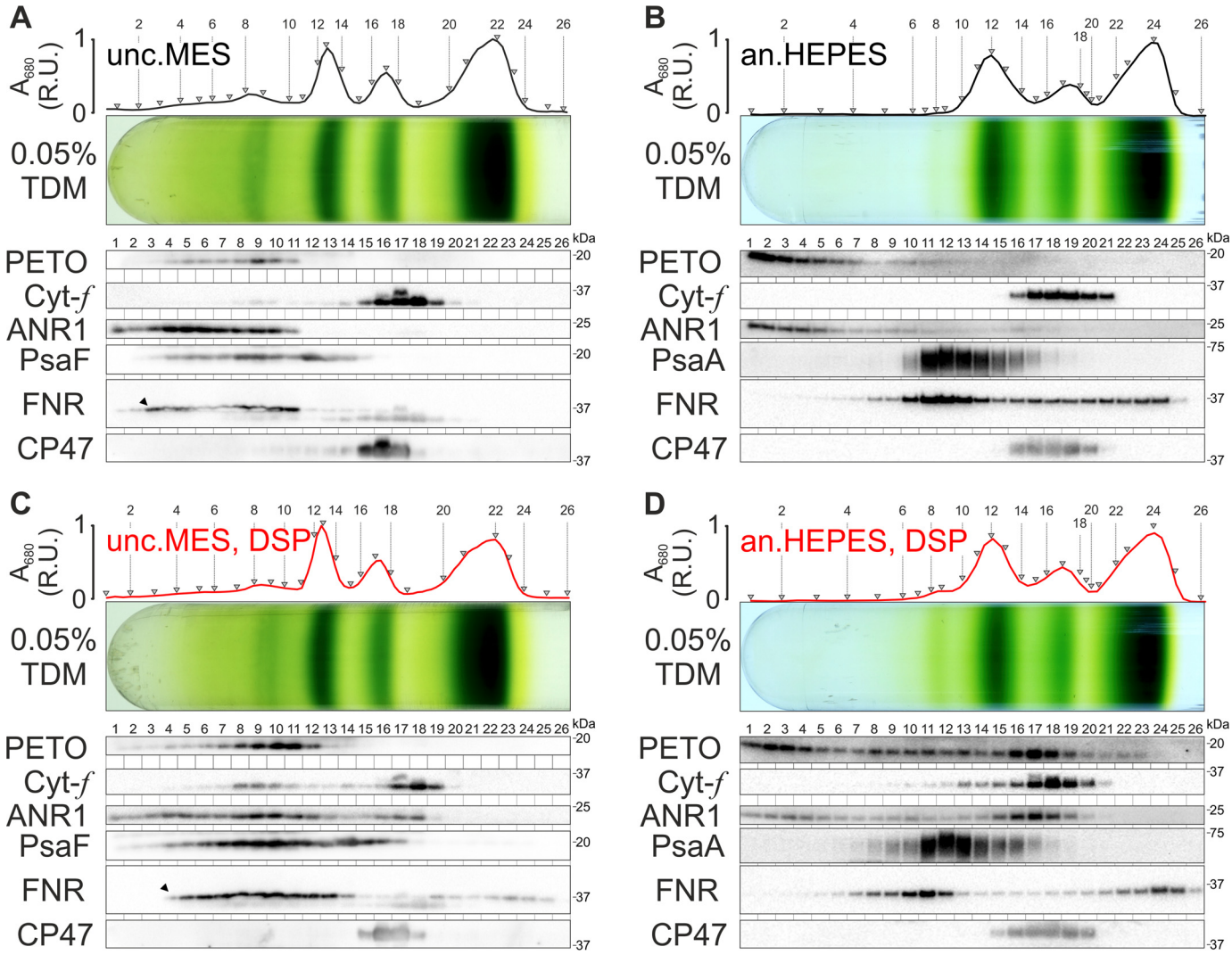


**Figure 3. Despite using different isolation protocols and the DSP cross-linker, comigration of PSI and Cyt-$b_6f$ in heavy SDG fractions was underrepresented.** State 2–inducing conditions and isolation buffers were either as in Iwai *et al.* (21) (*A* and *C*) (*unc.MES*, FCCP uncoupler incubation and MES buffers) or as in Takahashi *et al.* (18) (*B* and *D*) (*an.HEP*, anoxia and HEPES buffers). Cells were disrupted with a French press. Solubilization and sample loading was as in Fig. 1*A*. At variance, the SDG was supplemented with 0.05% TDM (w/v). Where indicated, 2.5 mM DSP was used as Lys cross-linker as under "Experimental procedures." *A*, the *densest green band* in fractions 7–10 contained PETO, ANR1, PSI (PsaF), FNR, and traces of Cyt-$b_6f$ (Cyt-*f*). PETO, ANR1, and FNR migrated *below* the major PSI band in fractions 11–15. The Cyt-$b_6f$ majority was in fractions 15–19. *B*, the an.HEP protocol without DSP pretreatment yielded *three green bands* and a *faint band* in fractions 7–9. PETO, ANR1, and Cyt-$b_6f$ distribution resembled that in *A*. The abundance of PSI (PsaA) was confined to the *major green band* in fractions 10–15, and FNR migration peaked with PSI while smearing to lower sucrose densities (up to *24*). *C*, the DSP pretreatment in unc.MES samples did not change the *green bands* but, compared with *A*, increased Cyt-$b_6f$ abundance in the *densest band* (fractions 7–10). Strong FNR signals were detected between fraction 5 and the PSI peak in fraction 13. Low-density fractions contained minor amounts of FNR (smearing up to *25*), PSI (up to *17*), and ANR1, which comigrated with the smearing PSI and Cyt-$b_6f$ majority (up to *18*). *D*, compared with *B*, DSP treatment produced a *greener band* in fractions 7–9, which contained minor populations of PSI and FNR. The FNR peak around fraction 11 was slightly displaced from the PSI peak (fractions 11–13). A DSP-dependent FNR peak at fractions 23–25 was produced. The Cyt-$b_6f$ majority remained in fractions 17–20, but traces were detected in higher sucrose densities (down to *9*). Both PETO and ANR1 were retained in low-density fractions comigrating with smearing PSI and peaking with Cyt-$b_6f$ majority. *R.U.*, relative units of normalized Chl absorbance at 680 nm.

plex protein distribution across the SDG, we observed a larger portion of Cyt-$b_6f$ now retained in high-density fractions 8–10, where PSI, PETO, ANR1, and FNR were also found (Fig. 3*C*).

When exploring the DSP effect in solubilized HEPES-buffered samples (Fig. 3*D*), the green intensity of fractions 7–9 showed a marked increase, due to the presence of minor but significant amounts of PSI in these higher-density fractions. However, these fractions only contained minute amounts of Cyt-$b_6f$, far from fulfilling the expectations for a CEF supercomplex.

The FNR detection in heavy fractions was not only dependent on the detergent concentration in the SDG (Fig. S4). As compared with untreated samples, DSP pretreatment increased FNR bimodal distribution due to the loss of signal in the Cyt-$b_6f$–containing fractions (Fig. 3, compare *B* and *D*). The DSP effect on bimodal FNR distribution was also seen in low-TDM SDG conditions (Figs. 2*A* and 4*A*; see assembly in Fig. S6). A large FNR proportion was found in higher-density SDG fractions, where a subpopulation of PSI also was found. This suggests that the destabilization of PSI–FNR interactions in low-TDM SDG was in part counteracted by the cross-linking treatment before solubilization. A most striking effect of the cross-link treatment was on ANR1 and PETO, which comigrated in SDG fractions with either PSI or Cyt-$b_6f$, thus pre-

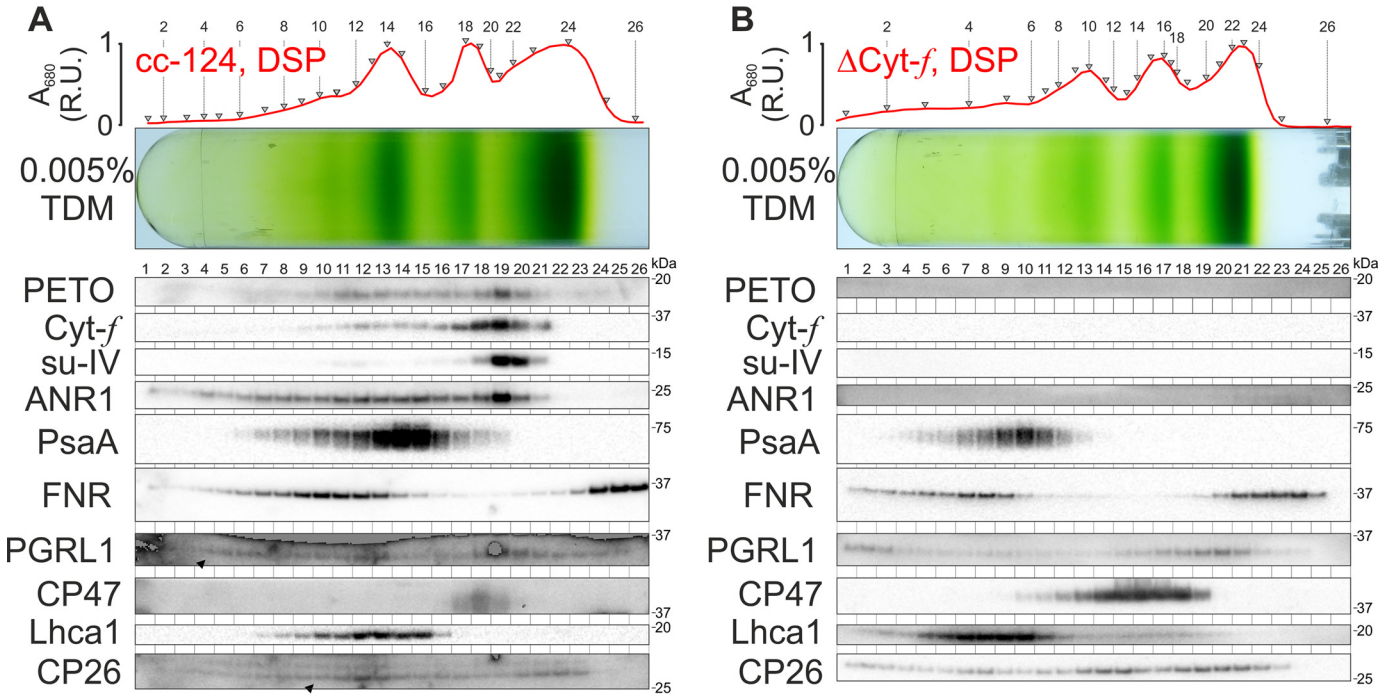


**Figure 4. DSP induced migration changes of green bands and CEF supercomplex components, which were partially Cyt-$b_6f$–independent.** The samples were isolated and analyzed as in Fig. 2 but pretreated with DSP as in Fig. 3*D*. Therefore, see Fig. 2 for the DSP effect and Fig. 3*D* for the high-TDM SDG effect in cc-124. *A*, the *green band* and protein migration profile of DSP-treated cc-124 thylakoids were changed in low-TDM SDG. The *heavy green band* (fractions 4–7 in Fig. 2*A*) disappeared, and a relative pigmentation increase of the PSI major band (fractions 12–16) was observed. The DSP effect on ANR1, PETO, and Cyt-$b_6f$ migration resembled high-TDM SDG (Fig. 3*D*). In addition to the low-density FNR peak in fractions 24–26 (see also Fig. 2*A*), the DSP effect on FNR produced high-sucrose density peak fractions 9–13, cofractionating with PSI but slightly offset to the PSI major band. DSP pretreatment broadened PGRL1 distribution. *B*, the DSP effect on the green band patterns in ΔCyt-*f* was identical to the WT, as were the changes in FNR distribution. *R.U.*, relative units of normalized Chl absorbance at 680 nm.

venting their aggregation in high-sucrose density fractions after their solubilization (see Figs. 2–4). In the following three sections, we will focus on these two proteins, which were hardly detectable in solubilized membranes of a Cyt-$b_6f$ mutant.

### *The effect of DSP on the SDG migration behavior of ANR1 and PETO is independent of the other auxiliary CEF protein*

ANR1 has been described as interacting with PETO (23), and indeed ANR1 and PETO had a strikingly similar migration behavior in the TDM-containing SDG, with and without DSP pretreatment. We also observed that the accumulation of ANR1 and PETO in whole-cell extracts was compromised in stationary cultures of two independent Cyt-$b_6f$–lacking mutant lines (Fig. S7). These experiments confirmed earlier reports on a Cyt-$b_6f$–dependent accumulation of PETO (23, 25, 26) and demonstrate a similar behavior for ANR1.

The DSP-treated WT sample in Fig. 4 showed SDG peak fractions of both ANR1 and PETO distribution where the major population of Cyt-$b_6f$ fractionated. Their low amount in the absence of Cyt-$b_6f$ (Figs. 2*B* and 4*B*) precluded further investigations on their migration upon SDG centrifugation in the total absence of this protein complex. We thus looked at whether the purported interactions of ANR1 and PETO with Cyt-$b_6f$ were mutually dependent. A ΔANR1 strain was available in the CLiP library, and PETO-knockdown strains were described previously (23). Fig. 5 shows the SDG centrifugation result of solubilized thylakoid membranes from these two mutants and demonstrates the effect of DSP treatment. It is apparent that the DSP-induced comigration of a subpopulation of either ANR1 or PETO with the Cyt-$b_6f$ did not require the participation of the other protein, meaning that their putative interactions with Cyt-$b_6f$ were independent from each other. In the following sections, we investigated these interactions by looking at possible cross-link events between ANR1 and PETO with the Cyt-$b_6f$.

### *Cross-link–assisted description of the PETO interface with Cyt-$b_6f$*

To understand whether mutually independent changes in ANR1/PETO migrations upon DSP pretreatment involved actual cross-links with Cyt-$b_6f$, we used the $H_6F_5$ strain, which harbored a modified Cyt-*f* fused with a $His_6$ tag at its C terminus (38) and followed the same isolation, cross-link, and solubilization protocol as for the WT and mutants in Fig. 5. Instead of analyzing samples via SDG ultracentrifugation, we used a two-step anion-exchange/metal-affinity purification protocol and examined the Cyt-$b_6f$ preparation on a nonreducing/reducing 2D PAGE, as shown in Fig. 6. This purification procedure has been used previously for crystallization of the algal Cyt-$b_6f$ core, which contained neither PETO nor ANR1 (27). A mix of antibodies to Cyt-*f*, su-IV, and PETO was used for immunoblotting the 2D gels in which cross-links were cleaved in the second dimension; thus, off-diagonal signals resulted from cross-links (or interprotein disulfides) in the first dimension. It is of note that proteins with covalent heme binding, cytochrome $b_6$ and Cyt-*f*, were readily detected by the enhanced chemiluminescence methods used for the immunoblots (39). As shown in Fig. 6*A*, PETO could not be detected with Cyt-$b_6f$ when omitting

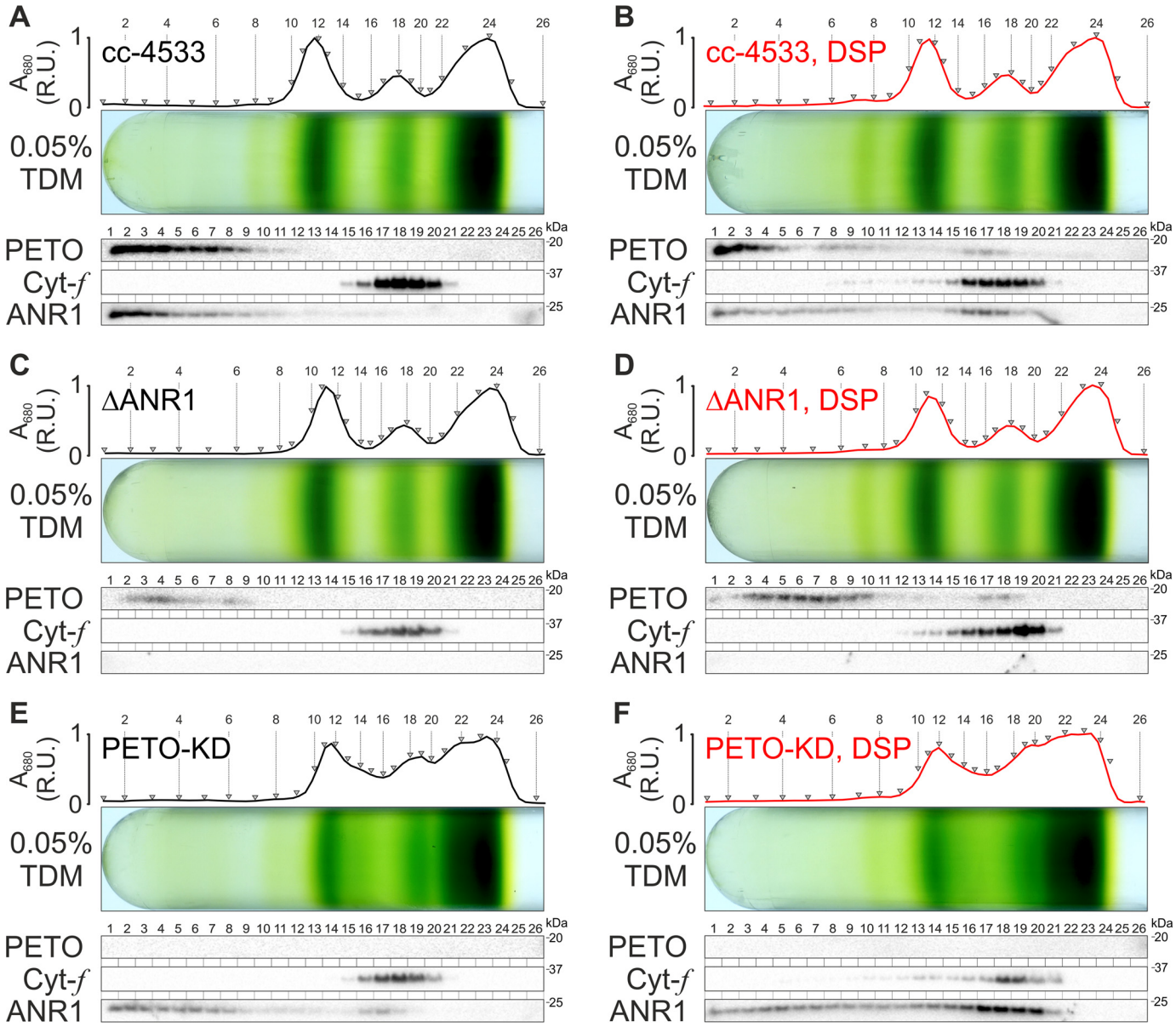


**Figure 5. DSP caused migration changes of ANR1 and PETO during SDG ultracentrifugation that did not rely on the presence of the respective other protein.** The conditions were as in Fig. 3 (*B* and *D*). The DSP-induced broadening of Cyt-$b_6f$ distribution in SDG was observed in cc-4533 WT in *A* and *B*, ΔANR1 (LMJ.RY0402.098359) in *C* and *D*, and the PETO-knockdown (*KD*) strain (23) in *E* and *F*. Upon cross-linking, comigration of PETO and ANR1 with the Cyt-$b_6f$ majority in fractions 16–20 (*B*) was independent of the respective other protein, because PETO comigrated with Cyt-$b_6f$ in the absence of ANR1 (*D*), and vice versa (*F*). *R.U.*, relative units of normalized Chl absorbance at 680 nm.

the DSP pretreatment of the thylakoids. On the contrary, PETO was easily detected in the DSP-treated samples, showing a cross-link with Cyt-*f* and su-IV (Fig. 6*B*; see legend for more details). These observations expand earlier studies that proposed PETO as a loosely attached algal Cyt-$b_6f$ subunit (25, 26).

Next, we submitted the affinity-purified Cyt-$b_6f$ DSP sample to MALDI-TOF/TOF. Before the measurements, the disulfide bridges were cleaved to identify which surface Lys residues were reproducibly labeled by DSP, yielding a variable Lys modification (+145.01975) from the carboxyamidomethylated, cleaved DSP in three biological replicates (Table S1). Because ionization efficiency of cross-linked peptides is often low, thus interfering with cross-link identification, the DSP-labeling approach gave us a first hint which Lys residues were easily reacting with the chemical. Ultimately, we attempted to identify the cross-linked residues with the ECL2 algorithm (40). Therefore, as outlined under "Experimental procedures," we used the noncleavable homobifunctional disuccinimidyl suberate (DSS) and thylakoid samples, which were solubilized with αDM. Similar to experiments with DSP, the Lys cross-linker DSS was added before solubilization. The ECL algorithm (40) deconvoluted the measured LC-MS/MS spectra of Cyt-$b_6f$–containing SDG fractions and identified cross-linked peptides from PETO and su-IV. We were not able to detect DSS-cross-linked peptides from PETO and Cyt-*f*. The LC-MS/MS spectra for peptides KPDLSDPVLkAK (PETO) and SENGVTFPkVAAGGTK (su-IV) with cross-linked Lys in lowercase type are shown in Fig. S8. By using RaptorX structure prediction

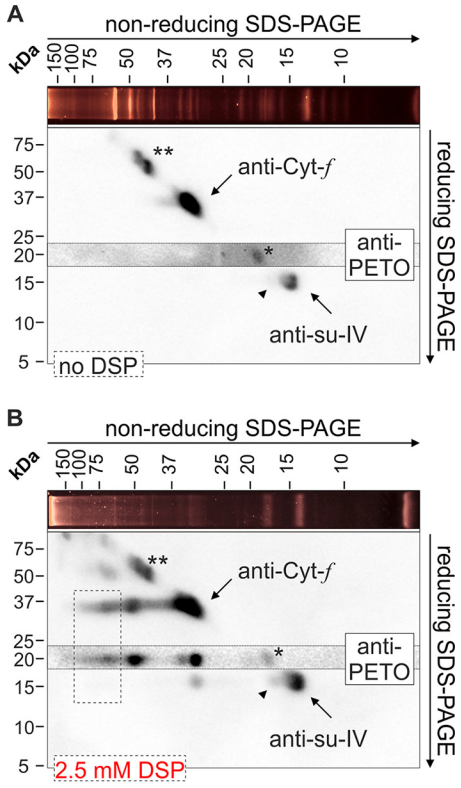


**Figure 6. PETO was copurified upon cross-linking to Cyt-$b_6f$ polypeptides cytochrome *f* and subunit IV.** The $H_6F_5$ strain with a C-terminal His tag on Cyt-*f* (38) was used for 2D SDS-PAGE (first dimension, nonreducing conditions with proteins stained by SYPRO Ruby; second dimension, reducing conditions, blotted on nitrocellulose). *A*, the purification protocol did not yield sufficient PETO amounts to be detected on Western blotting without DSP pretreatment, whereas peroxidase activity of hemes in cytochrome $b_6$ (*) and Cyt-*f* aggregates (**) produced chemiluminescence signals. The *arrowhead* marks a putative disulfide between Cys-50 of su-IV and Cys-18 of PetN. *B*, DSP addition before solubilization produced PETO signals that comigrated with su-IV and Cyt-*f* in the first dimension by preserving interactions when Lys–Lys cross-links were established. The *dashed box* indicates simultaneous PETO cross-links with both Cyt-$b_6f$ subunits, at the immunodetection limit of the su-IV antibody.

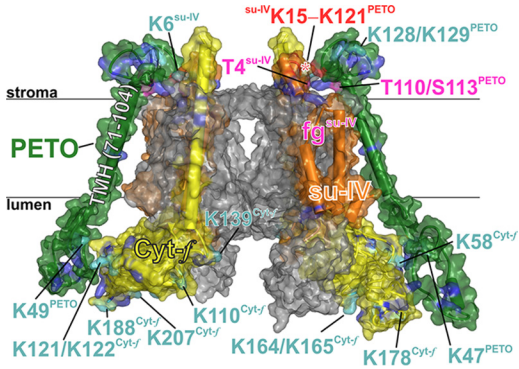


**Figure 7. Structural PETO model cross-linked to subunit IV of the Cyt-$b_6f$.** The position of the cross-link (*red asterisk*) on the *orange* su-IV is shown in the homodimer assembly of Cyt-$b_6f$, taken from Protein Data Bank entry 1Q90 (27). The corresponding MS2 spectrum is shown in Fig. S8. A model structure of PETO (*green*) was generated using the RaptorX service (41) with manual refinement of the transmembrane helix (*TMH*; residues 71–104). The Cyt-*f* polypeptide is shown in *yellow*, and the remaining subunits are shown in *gray*. The transmembrane helices in the su-IV, Cyt-*f*, and PETO models are depicted as *solid cylinders*, and simplified loops were overlaid by a *semitransparent surface representation*. Various lumenal PETO and Cyt-*f* residues were DSP-labeled (*cyan*; see Table S1), but cross-links could not be identified, and Lys residues that were not labeled are shown in *blue*. *Pink* STT7-related elements in proximity to the lumenal cross-link highlight phosphorylation sites in PETO and su-IV (28) as well as a putative STT7 interaction interface located in the stromal su-IV loop, $fg^{su\text{-}IV}$ (42).

server (41), a PETO model was placed in proximity to the published structure of *Chlamydomonas* Cyt-$b_6f$ (27). PETO was reported to have a lumenal N terminus that is separated from the stromal C terminus by a single transmembrane helix (25). Interestingly, the C terminus of PETO was cross-linked to the stromal N terminus of su-IV through their respective lysines, Lys-121 and Lys-15 (Fig. 7). This cross-link develops in close vicinity of the Ser/Thr kinase STT7-dependent phosphorylation sites Thr-110 and Ser-113 of PETO and Thr-4 of su-IV (28). It is notable that a nearby peripheral stromal loop, formed by su-IV residues 113–128, interacts with STT7 (42).

### *ANR1 is not cross-linked to the Cyt-$b_6f$ by DSP, but they cofractionate in the amphipol-trapped state*

By following the approach described for PETO in Fig. 6, we failed to detect any cross-link supporting ANR1 as an interaction partner of the affinity-tagged Cyt-$b_6f$ in the $H_6F_5$ strain. This is consistent with the immunoblot of a DSP-treated sample probed with an antibody to ANR1 (Fig. 8*A*). The absence of an ANR1 cross-link with Cyt-$b_6f$ appears to conflict with their DSP-induced comigration in SDG (*e.g.* see Fig. 5*F*). We then assumed that not ANR1 itself but an unknown interactor(s) would be cross-linked to Cyt-$b_6f$. The unknown Cyt-$b_6f$ cross-link partner(s) only interacts with ANR1 at low ionic strength and gradually detaches from TDM-solubilized Cyt-$b_6f$ during the lengthy SDG ultracentrifugation. Using an anion-exchange step (27) that resembled CEF supercomplex–destabilizing conditions (21) during the Cyt-$b_6f$ purification procedure could therefore wash away ANR1 even upon DSP pretreatment. To test these assumptions, we searched for better conditions to stabilize protein/protein interactions between detergent-solubilized proteins. We used a PETO-Strep tag strain as well as trapping of TDM-solubilized proteins by amphipols.

The PETO-Strep strain allowed purification of Cyt-$b_6f$ complexes at slightly less harsh conditions regarding the ionic strength (170 mM instead of 250 mM NaCl). This strain had been designed in a previous study to show that, among CEF-involved proteins, ANR1 was the main interactor of PETO (23). Whereas we could reproduce a limited ANR1/PETO coelution in the control experiment, DSP pretreatment increased the abundance of Cyt-$b_6f$, but not of ANR1, in the batch-eluted PETO fractions (Fig. 8*B*). At variance with the previous report (23), FNR remained below detection in the eluted fractions in our experimental conditions. As a control, none of the above proteins were detected in the elution fractions using strains that overexpressed WT PETO (Fig. S9).

We tested whether minimizing exposure time to TDM could stabilize ANR1-specific Cyt-$b_6f$ interactions. It has been observed previously that Cyt-$b_6f$ homodimers disassemble over time in certain maltoside detergents (43, 44). Therefore, we used the amphipol PMal-C8 in a second approach (45, 46). These short amphipathic surface-active agents can substitute for detergents, thus creating stabilizing interactions of various solubilized MPs (reviewed by Zoonens and Popot (31)). However, the amphipol capacity to solubilize MPs is poor, and

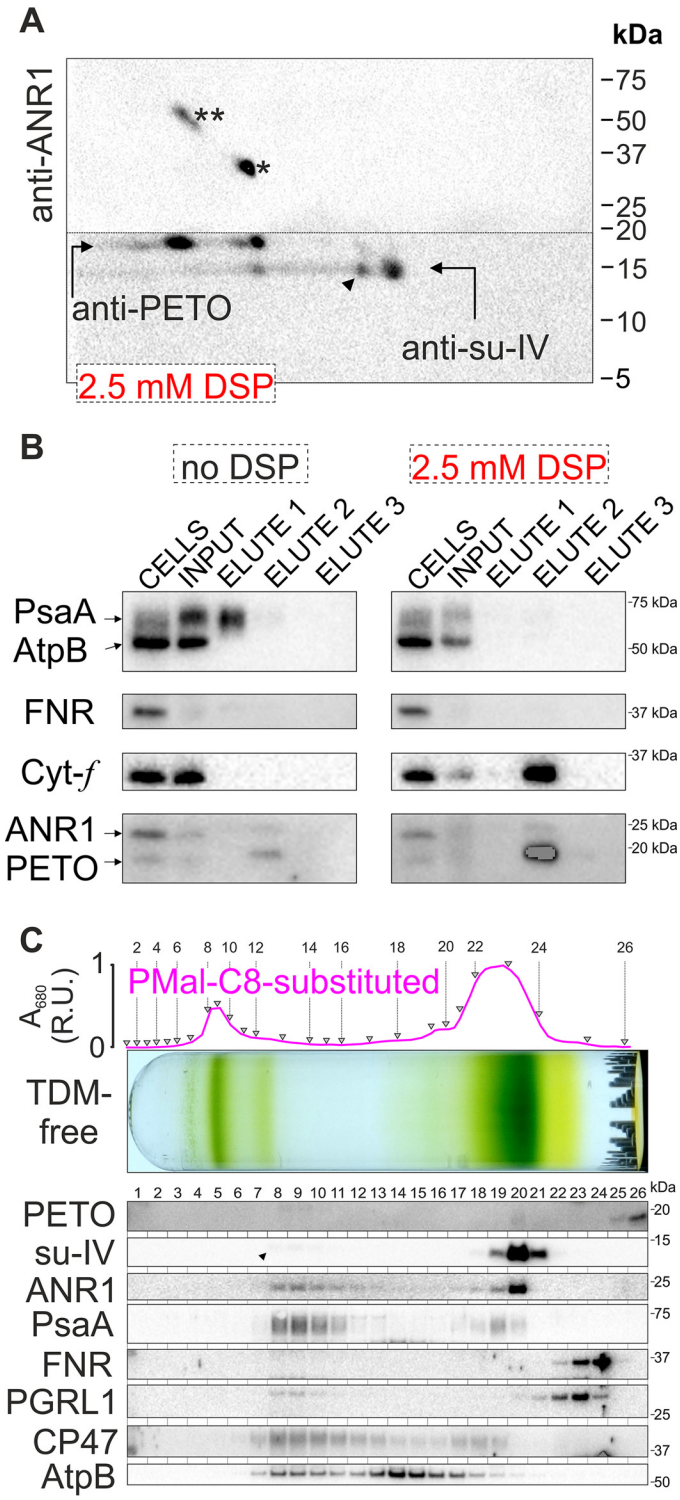


**Figure 8. ANR1 was not enriched with Cyt-$b_6f$/PETO upon cross-linking but comigrated with Cyt-$b_6f$ in an amphipol-stabilized state without cross-linking.** *A*, the $H_6F_5$ strain was used for 2D SDS-PAGE as in Fig. 6. Immunodetections of a DSP-treated sample in the second dimension are shown and did not yield detectable signals for ANR1 in the upper half of the blotted membrane at ~25 kDa. The hemes in Cyt-*f* (*) and Cyt-*f* aggregates (**) produced chemiluminescence signals. The *arrowhead* marks a putative disulfide between Cys-50 of su-IV and Cys-18 of PetN. *B*, the PETO-Strep tag–overexpressing strain (23) served in an unsuccessful attempt to retain indirect ANR1-Cyt-$b_6f$ interaction(s) upon DSP treatment. Total cell extracts (0.5 $\mu$g of Chl) were loaded, and the input load was soluble supernatant volumes equivalent to 0.5 $\mu$g of Chl before solubilization. The sample load volumes for three 1-ml batch elution fractions were the same. DSP pretreatment reduced the amount of solubilized MP and facilitated Cyt-$b_6f$ copurification, but failed to enrich ANR1. *C*, TDM-solubilized cc-124 thylakoids were incubated with polystyrene beads to remove the detergent in the presence of the amphipol PMal-C8. After spinning down briefly, 375 $\mu$l of the supernatant were ultracentrifuged in an SDG devoid of TDM, yielding a low-density PETO fraction 26 and comigration of Cyt-$b_6f$ and ANR1 in fraction 20. Heavy SDG fractions contained minute amounts of Cyt-$b_6f$, indicated by the *arrowhead*. *R.U.*, relative units of normalized Chl absorbance at 680 nm.

therefore a detergent-mediated solubilization is necessary. By choosing the buffer composition (46, 47) and adding an excess of PMal-C8 during detergent removal (see "Experimental procedures"), we favor the coverage of hydrophobic protein domains by the zwitterionic amphipol while disfavoring electrostatic and/or hydrophobic protein aggregation processes in the detergent-free solution. Even if the latter artifact existed, it was eliminated by the centrifugation step before supernatant loading. The samples shown in Fig. 8*C* were solubilized by TDM, followed by substitution with PMal-C8 and TDM removal. After spinning down the mixture, the supernatant was loaded on an SDG that was not supplemented with TDM. The samples now contained the solubilized photosynthetic machinery with PSI and PSII showing a bimodal distribution upon SDG centrifugation. PSI showed two defined populations (fractions 8–13 and 18–20), as did PSII, peaking in fractions 8–11 and 17–19. Fractions 8–11 also showed minute amounts of Cyt-$b_6f$ (*arrowhead* in Fig. 8*C*), which accumulated mostly in fractions 19–21. Interestingly, ANR1 now peaked together with Cyt-$b_6f$ in fraction 20, which suggested stabilization of the ANR1/*X*/Cyt-$b_6f$ interface in the detergent-free state. Here, *X* refers to the unknown Cyt-$b_6f$-cross-linkable protein(s), as assumed above in the TDM detergent system. Fraction 20 contained only trace amounts of PETO. The latter was mostly detected in the upper fractions 25–26, at moderate sucrose densities that correlated with its apparent molecular weight. Significant amounts of ANR1 were also detected in the high-sucrose density fractions 8–11, as were PSI (PsaA), PSII (CP47), PGRL1, and the ATP synthase (AtpB). The slight relative offset migration of CEF effectors FNR and PGRL1 in the upper region was also observed in low-TDM SDG (Fig. 2*A* and Fig. S1).

## Discussion

Here we provided a molecular characterization of the Cyt-$b_6f$ interaction with the loosely attached CEF effector PETO. PETO was cross-linked to either su-IV or Cyt-*f*, rather than producing a cross-linked tripeptide. This raises the question of the actual PETO stoichiometry per Cyt-$b_6f$. The following attempts to compensate the missing PETO-Cyt-*f* cross-link identification and explain Fig. 6*B* are summarized in Fig. 9*A*. Disregarding higher stoichiometries, PETO isoform-specific cross-links could occur in the case of two PETO per functional Cyt-$b_6f$ homodimer (PETO/Cyt-$b_6f$ ratio of 1). When assuming a ratio of 0.5, two scenarios are possible. (i) Supported by reproducible DSP reactivity of various lumenal Lys residues in Cyt-*f* and PETO, it is likely that there was a yet-to-be-pinpointed *lumenal* PETO-Cyt-*f* cross-link. Upon PETO cross-linking on one side of the membrane (to *stromal* su-IV or *lumenal* Cyt-*f*), structural alterations in PETO are transmitted to the opposite side of the membranes, which hamper subsequent cross-links on that side.

In this view, Fig. 6*B* would be a *stochastic snapshot* of the PETO/Cyt-$b_6f$ population. Signal transduction across the membrane indeed has been suggested for other proteins, such as the STT7 kinase (48). STT7 is important for state transition, which is a CEF-independent process to optimize photosynthesis under suboptimal conditions (18) (reviewed by Rochaix *et al.* (49)). STT7 was shown to interact with the Cyt-$b_6f$ (42) and relies on both the redox state of the PQ pool (50) and a functional, lumenal $Q_o$ site of the Cyt-$b_6f$ (35) opposite to the stromal site where the catalytic activity of the kinase takes place. (ii) An alternative to cross-link–mediated alterations in PETO across the membrane would be that of an STT7-induced phosphorylation of stromal Ser/Thr in both PETO and su-IV, which have been identified in proximity to our reported cross-link site (28). These posttranslational modifications could reorganize salt bridges and other electrostatic networks (51), which would then favor *stromal* PETO-Cyt-*f* interactions as well. Here, Fig. 6*B* would be a *metabolic snapshot* of the PETO/Cyt-$b_6f$ population. Even without further elaborating on the yet-to-be-identified Cyt-$b_6f$/ANR1 interface and autophosphorylation of the STT7 kinase domain that results from the interaction with a proximal su-IV loop of Cyt-$b_6f$ (42), the suggested stromal scenario involves highly dynamic and partially competing protein interactions. These processes could participate in CEF and/or state transition regulation.

Because ANR1 and PETO are algae-specific CEF effectors (22, 23), they might play a role in CEF features that are not found in higher plants. *Chlamydomonas* has a versatile anaerobic metabolism (52, 53), and the lack of oxygen induces several anaerobic responses like increased ANR1 expression (24) and increased CEF due to an altered PQ pool redox equilibrium (18, 22, 23). Algal and plant PQ pool redox equilibria differ due to changes in chlororespiration, which is electrogenic in plants only (reviewed by Nawrocki *et al.* (7)). It has been documented that plant type-1 NDH can use Fd as electron donor (54), which may not be the case for the algal type-2 NAD(P)H dehydrogenase (5). Recently, ANR1 was shown to share a motif with NdhS, which is the Fd-binding subunit in plant NDH (23). Interestingly, both ANR1 and PETO interact with Fd FDX1 (55). ANR1 also develops specific FDX2 interaction, whereas PETO interacts with FDX5 (56). Thus, the two algal CEF effectors could be Fd-shuttling proteins between PSI and Cyt-$b_6f$, the latter acting as an Fd-PQ reductase (Fig. 9*B*). In this view, Cyt-$b_6f$ receives Fd from PETO/ANR1 via FNR, which was shown to bind plant Cyt-$b_6f$ (13, 14). It should be noted that FNR in *Chlamydomonas* is encoded by a single gene only, unlike in plants that express multiple isoforms with specific membrane association preferences (14, 57). Algal FNR is bound to the membrane in a PGR5-dependent manner (58). Its membrane tethering differs in general because higher plant FNR-binding proteins are missing in *Chlamydomonas* (59–61). Presently, we do not know whether PGRL1/PGR5 contribute to FNR tethering in algae directly or play a role in a quality control of the FNR pool that participates in CEF and LEF.

Although the cross-link–assisted disintegration analysis enabled us to identify further CEF-related protein interactions, we conclude that the commonly applied SDG approach, due to its liability to artifacts, is not appropriate for further biochemical characterization of the CEF supercomplex. Chl-containing heavy SDG fractions can easily be misidentified with the putative CEF supercomplex. Its isolation would require, for instance, an additional affinity chromatography purification step to demonstrate genuine interactions between comigrating proteins. Unfortunately, the buffers that ensure specific binding to the immobilized phase also promote disruption of the CEF supercomplex (21).

SDG served as a tool to separate solubilized MP complexes of different apparent molecular weight. However, there is no straightforward correlation between their migration behavior and their molecular weight because shape, density, and hydrophobic interactions also contribute to their behavior upon SDG centrifugation. Here we observed that, when (in)directly cross-linked to Cyt-$b_6f$ assemblies, PETO and ANR1 were retained in

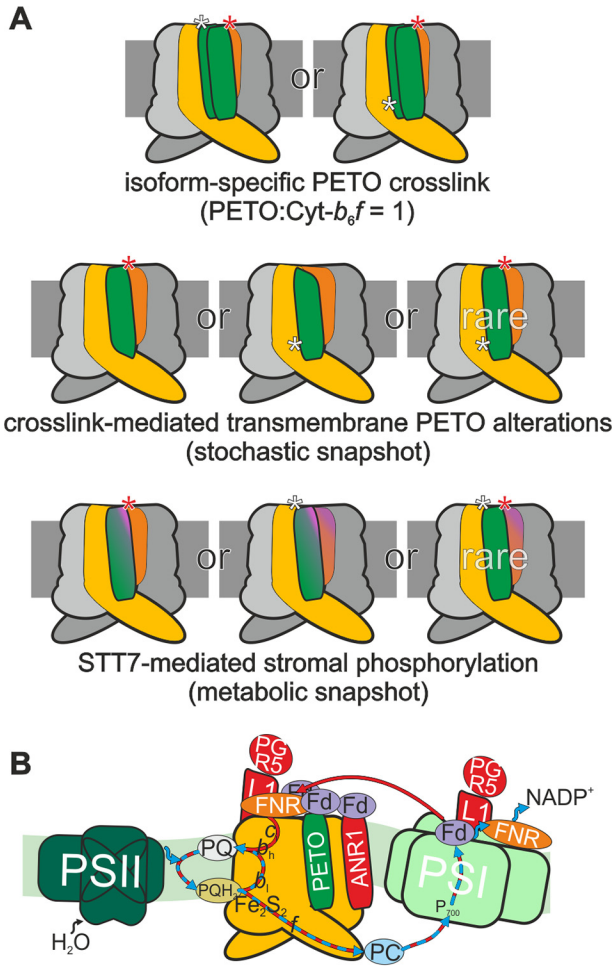


**Figure 9. Various possible Cyt-$b_6f$/PETO cross-link scenarios and proposed function of Cyt-$b_6f$-interacting CEF effectors ANR1 and PETO.** *A*, the *cartoon* of Cyt-*f* (*yellow*), su-IV (*orange*), and PETO (*green*) places the detected cross-links from Fig. 6*B* in the context described under "Discussion." The cross-link sites were identified (*red asterisk*) or suggested (*white asterisk*). STT7-dependent phosphorylation is marked in *magenta*. *B*, a *cartoon model* of CEF (*red arrows*) is shown. LEF is depicted with *blue arrows*. The FNR is tethered to the membrane dependent on PGRL1 (L1) and PGR5 (58). Bound to Cyt-$b_6f$ (*yellow*; marking $f/b_l/b_h/c_i$ hemes and Rieske $Fe_2S_2$ protein), the FNR injects electrons into the PQ pool via heme $c_i$ (13–15). Our study proposes Fd-shuttling functions of ANR1 and PETO (55, 56) during this process by interacting with the Cyt-$b_6f$. As outlined under "Discussion," the CEF supercomplex model proposed by Iwai *et al.* (21) requires improved protocols to be further validated and/or characterized.

lower-sucrose density fractions. Compared with the control, relative SDG migration of the ~220-kDa Cyt-$b_6f$ homodimer was not altered. This was unexpected because of the apparent gain in molecular mass of the Cyt-$b_6f$ homodimer assembly by at least 35 kDa, depending on the actual (yet unknown) CEF effector ratio per Cyt-$b_6f$. Other unexpected SDG results were related to solubilization processes during the rate-zonal centrifugation step. Accordingly, the behavior of FNR was odd when changing the TDM concentration in the gradients. Considering the various parameters that participate in the solubilization process (30), the membrane-peripheral FNR co-solubilized with PSI and/or Cyt-$b_6f$ in high-TDM SDG (0.05% TDM), probably because FNR binding to its CEF sites or to tethering proteins was inaccessible at low-TDM SDG (0.005% TDM). Thus, optimal detergent conditions for tethering FNR to a CEF supercomplex interfered with stable core component assemblies (43, 44) during lengthy rate-zonal centrifugation steps. Keeping integral MP complexes in their original oligomeric state, outside their natural environment, remains a major biochemical challenge (reviewed by Seddon *et al.* (30)), particularly when facing loose interactions as in the CEF supercomplex. The presence of CEF effectors in heavy fractions at the bottom of TDM-SDG, previously considered to represent either TDM-inaccessible membrane microdomains or high-molecular weight complexes (23), could in fact be interpreted as MP aggregates. When stabilizing TDM-solubilized MP by trapping with amphipol PMal-C8, we observed a striking co-fractionation of ANR1 with the Cyt-$b_6f$ homodimer. The amphipol-stabilized CEF effectors PETO, PGRL1, and FNR, which we routinely detected in high-sucrose density fractions or smearing across the TDM-SDG, also migrated in well-defined regions in a detergent-free state. In conclusion, the heavy, detergent-containing SDG fractions contained broadly migrating CEF effector aggregates and the purported CEF supercomplex core. Regarding fractionation of the latter, PSI and Cyt-$b_6f$ signal intensities were poorly correlating. Therefore, further purification steps of the pooled fractions of interest are crucial. These will, however, increase the chances of additional destabilization. Using subsequent affinity chromatography allowed us to purify putative CEF supercomplexes from SDG at very low yield (73), suggesting the development of novel purification protocols of the labile CEF complex. In that respect, amphipols might be an additional promising approach for future CEF supercomplex research. Furthermore, alternative methods like interval zone free-flow electrophoresis will also facilitate further biochemical progress. Using this technique in *Arabidopsis thaliana*, Cyt-$b_6f$/PSI particles were observed recently (62).

Taken together, we conclude that the published CEF supercomplex isolation procedures need further improvement to assess their actual existence and to proceed with functional and structural characterization because the MP assemblies are easily destabilized using previous protocols. Our results demonstrate mutually independent interactions between the two Fd-interacting CEF effectors ANR1 and PETO with the Cyt-$b_6f$ in *C. reinhardtii*. Based on our current observations, we favor the concept proposed by Joliot *et al.* (15), where Cyt-$b_6f$-associated FNR (13, 14) facilitates the reinjection of electrons at the $Q_i$ site via heme $c_i$. During this process, the CEF effectors PGR5/PGRL1 and ANR1/PETO likely play FNR-coordinating (58) and Fd-coordinating roles (55, 56) that are functionally redundant because none of the single knockout/knockdown strains is truly CEF-impaired (12, 22, 23, 63).

## Experimental procedures

### Chemicals

Unless stated, all chemicals were purchased from Sigma-Aldrich. TDM (AppliChem, Darmstadt, Germany), αDM (Biomol GmbH, Hamburg, Germany), PMal-C8 (Anatrace, Maumee, OH), trypsin/Lys-C mix (Promega), SYPRO Ruby, Pierce ECL Western blotting substrate, DSP, and DSS (Thermo Fisher Scientific) were purchased from elsewhere.

### Strains and growth conditions

In the experiments, *C. reinhardtii* WT cc-124 (nit2$^-$, mt$^-$) and cc-4533 (cw15 mt$^-$) were used. The latter was provided as reference for ΔANR1, which was an insertional mutant (locus Cre03.g164000) designated as LMJ.RY0402.098359 in the CLiP library (64). Strains that overexpressed PETO (WT or coding for Strep-tagII) and the PETO-knockdown strain 3B8 were described previously (23) and generated in the *arg7* background (65). The $H_6F_5$ strain coded for a $His_6$-tagged Cyt-*f* (38). Cyt-$b_6f$–lacking strains Δf on the level of *petA*/Cyt-*f* (66) and Fud6 on the level of *petD*/su-IV (67) have been described previously. All cells were grown in Tris acetate phosphate (TAP) medium at 25 °C under 50 μmol of photons $m^{-2}$ $s^{-1}$ and kept in the exponential phase by repeated dilution in fresh TAP.

### State 2 induction and thylakoid isolation

Cells in the early to mid-log phase were harvested (5 min at 5000 rpm in Beckman JA-12 rotor, 22 °C) and resuspended in spent TAP medium to a density of ~5 × $10^7$ cells/ml. State 2 induction relied on oxygen removal either by incubating the harvested cells (15–25 ml) in the dark with 5 μM FCCP (21, 68) or bubbling with argon gas (22, 28) for ~45 min. The latter is referred to here as "anoxic conditions." State 2 transition was routinely checked by recording low-temperature fluorescence emission spectra at 77 K (not shown), followed by cell disruption either with a French press (18) at ~20 kilopascals or nebulization twice with a BioNeb cell disruptor at ~10 kilopascals (68). The thylakoid isolation was basically as described previously (34, 69), and CEF supercomplex studies were further modified from the original protocols (18, 21, 22). After French press or nebulizer passage, samples were handled throughout at 4 °C, and disrupted cells were diluted 1:1 in a prechilled 2× buffer, yielding a final mix of 25 mM HEPES (pH 7.5), 0.33 M sucrose, 10 mM EDTA, 10 mM NaF, 1.5 mM KCl, 5 mM 6-aminocaproic acid, 1 mM benzamidine, 1 mM phenylmethylsulfonyl fluoride (H25 buffer). Where indicated, HEPES was replaced by 25 mM MES, pH 6.5 (M25 buffer). Cells were pelleted (20 min at 40,000 rpm in a Beckman Type 45 Ti rotor) and homogenized in H5/M5 buffer using a potter. The H5/M5 buffer was identical to H25/M25 but only weakly buffered at 5 mM in the presence of 1.8 M sucrose. Thylakoid floatation via a three-step sucrose gradient was as described previously (69), and thylakoids were

resuspended in sucrose-free H5/M5 buffer devoid of 6-aminocaproic acid and benzamidine. For further use, the Chl concentration (70) was set to 2 and 1 mg/ml for experiments with and without the cross-link step, respectively.

### *Cross-link reactions*

DSP and DSS are homobifunctional and membrane-permeable cross-linkers. Both compounds contain amine-reactive *N*-hydroxysuccinimide esters at each end of an 8-carbon spacer arm (distance: DSP, ~12.0 Å; DSS, ~11.4 Å), thus cross-linking side chains of Lys. Chemical protein cross-linking was performed at 2.5 mM DSP or DSS. Thylakoids were diluted to a final concentration of 1 mg Chl/ml with freshly prepared cross-linker, added from a prewarmed 2× stock solution (2% (v/v) DMSO in sucrose-free H5/M5 buffer for mock controls). Cross-linking was carried out in the dark for 2 h on rotating disks. After 15-min quenching of nonreacted cross-linker with 50 mM Tris-HCl, pH 6.8, samples were solubilized.

### *Thylakoid membrane solubilization and SDG ultracentrifugation*

Thylakoids, equivalent to 1 mg of Chl/ml (or 0.95 mg of Chl/ml in cross-link experiments) were brought to 0.8 mg of Chl/ml by solubilizing in 0.85% (w/v) TDM for 20 min. TDM was added to the thylakoids from a 4.25% stock (5.38% in cross-link experiments), and during solubilization, the reaction tubes were inverted once every 4–5 min, unless otherwise stated. Before loading 375 $\mu$l of supernatant on the SDG, samples were spun down for 5 min at 14,000 rpm. The SDG (a discontinuous step gradient with 1.7/1.5/2.0/2.0/2.0/1.0 ml of 1.3/1.0/0.85/0.7/0.65/0.4 M sucrose) contained 5 mM Tricine-KOH (pH 8.0) and either 0.005 or 0.05% (w/v) TDM. Upon reaction, cross-links were present during SDG ultracentrifugation and cleaved in selected SDG fractions by incubation with 50 mM DTT for 1 h at 37 °C, followed by SDS-PAGE (71) and Western blotting, using a ChemiDoc imager (Bio-Rad).

### *Amphipol trapping*

Floated thylakoids were resuspended in 5 mM Tricine-KOH (pH 8.0), 10 mM EDTA, 5 mM 6-aminocaproic acid, 1 mM benzamidine, 1 mM phenylmethylsulfonyl fluoride and brought to 1 mg Chl/ml. After 10 min of solubilization as described above, the amphipol (50 mg/ml stock in 20 mM Tricine-KOH, pH 8.0, 10 mM EDTA) was added at a PMal-C8/Chl ratio of 7.5/1 (w/w), and the mix was incubated for another 20 min, followed by a 5-min centrifugation at 14,000 rpm. To remove the residual 0.76% TDM (w/v) from the supernatant, Bio-Beads$^{TM}$ SM-2 (Bio-Rad) were added at a 40-fold excess (by weight) and incubated for 2 h. The detergent-free SDGs were loaded with amphipol-trapped MP, equivalent to ~420 $\mu$l of solubilized thylakoids.

### *Affinity purification protocols*

The His-tagged Cyt-$b_6f$ (27) and Streptactin-tagged PETO (23) were purified according to previously published protocols using HiTrap Q HP and HisTrap HP columns for the former and Strep-trap HP columns for the latter (GE Healthcare). The His-tagged Cyt-$b_6f$ (15 $\mu$g of protein) was analyzed in nonreducing conditions in the first dimension, optionally stained by SYPRO Ruby, and gel slabs were incubated with 50 mM DTT for 1 h at room temperature, followed by SDS-PAGE in the second dimension and Western blotting.

### *Mass spectrometry analysis*

For in-gel digestion of the DSP labeling experiments, samples were reduced in 10 mM DTT and 50 mM $NH_4HCO_3$ for 30 min at 56 °C in darkness, followed by alykation in 50 mM iodoacetamide and 50 mM $NH_4HCO_3$ for 30 min at 56 °C in darkness. Trypsin digestion was performed overnight at 37 °C. The extracted peptides were then dried in a SpeedVac and resuspended in 40 $\mu$l of UPLC loading buffer (3% acetonitrile, 0.1% formic acid). For LC-MS/MS analysis, samples were analyzed by Nano LC-MS/MS using an EASY-nLC 1000 liquid chromatography system coupled to a Q Exactive plus mass spectrometer (Thermo Fisher Scientific). See Table S2 for details on LC and MS settings. MASCOT (Matrix Science, London, UK) interrogation was performed via the protein identification software Proteome discoverer (Thermo Scientific) with *C. reinhardtii* Uniprot DB. The search parameters allowed for up to three missed cleavages. Modifications with a peptide mass tolerance of 10 ppm were set as fixed for carbamidomethyl of Cys. Met oxidation, 3-(carbamidomethylthio)propanoyl of Lys, and protein N terminus were selected as variable modifications. Mass tolerances were 10 ppm on the precursor level and 0.02 Da on the MS2 level. False discovery rates for protein identification were fixed at 0.01. For cross-link site identification, isolated thylakoids were cross-linked with DSS and solubilized with $\alpha$DM. After an SDG ultracentrifugation, the Cyt-$b_6f$ fraction was tryptically digested using the FASP method (72). Peptides were then analyzed on an LC-MS/MS system consisting of an Ultimate 3000 nano-LC coupled to a Q Exactive Plus mass spectrometer (Thermo Fisher Scientific). See Table S2 for details on LC and MS parameters. The cross-linked peptide combination was found in multiple spectra that were evaluated with an ECL algorithm (40) using a *C. reinhardtii* Uniprot DB limited to chloroplast-localized proteins. Carbamidomethylated cysteine and oxidized methionine were set as fixed and variable modifications, respectively. Mass tolerances were as described above. Results were filtered to satisfy a false discovery rate of 0.01. The spectrum was plotted with ECL viewer version 2.0.

*Author contributions*—F. B. and F. -A. W. designed experiments; F. B. and P. G. performed biochemical experiments; M. Hamon, M. S., and M. Hippler designed MS experiments and analyzed MS data; F. B. and F. A. W. wrote the manuscript.

*Acknowledgments—We are thankful for the valuable help of Daniel Picot and Francesca Zito ($H_6F_5$), as well as Manuela Zoonens (amphipol) and Olivier Vallon (ΔANR1). The Proteomic Platform of IBPC (PPI) was supported by CNRS Grant EQUIPEX CACSICE ANR-11-EQPX-0008.*

**References**

1. Arnon, D. I. (1959) Conversion of light into chemical energy in photosynthesis. *Nature* **184,** 10–21 CrossRef Medline

2. Foyer, C. H., Neukermans, J., Queval, G., Noctor, G., and Harbinson, J. (2012) Photosynthetic control of electron transport and the regulation of gene expression. *J. Exp. Bot.* **63,** 1637–1661 CrossRef Medline
3. Bennoun, P. (1982) Evidence for a respiratory chain in the chloroplast. *Proc. Natl. Acad. Sci. U.S.A.* **79,** 4352–4356 CrossRef Medline
4. Shikanai, T., Endo, T., Hashimoto, T., Yamada, Y., Asada, K., and Yokota, A. (1998) Directed disruption of the tobacco *ndhB* gene impairs cyclic electron flow around photosystem I. *Proc. Natl. Acad. Sci. U.S.A.* **95,** 9705–9709 CrossRef Medline
5. Jans, F., Mignolet, E., Houyoux, P. A., Cardol, P., Ghysels, B., Cuiné, S., Cournac, L., Peltier, G., Remacle, C., and Franck, F. (2008) A type II NAD(P)H dehydrogenase mediates light-independent plastoquinone reduction in the chloroplast of *Chlamydomonas*. *Proc. Natl. Acad. Sci. U.S.A.* **105,** 20546–20551 CrossRef Medline
6. Trouillard, M., Shahbazi, M., Moyet, L., Rappaport, F., Joliot, P., Kuntz, M., and Finazzi, G. (2012) Kinetic properties and physiological role of the plastoquinone terminal oxidase (PTOX) in a vascular plant. *Biochim. Biophys. Acta* **1817,** 2140–2148 CrossRef Medline
7. Nawrocki, W. J., Tourasse, N. J., Taly, A., Rappaport, F., and Wollman, F. A. (2015) The plastid terminal oxidase: its elusive function points to multiple contributions to plastid physiology. *Annu. Rev. Plant Biol.* **66,** 49–74 CrossRef Medline
8. Joliot, P., Béal, D., and Joliot, A. (2004) Cyclic electron flow under saturating excitation of dark-adapted *Arabidopsis* leaves. *Biochim. Biophys. Acta* **1656,** 166–176 CrossRef Medline
9. Munekage, Y., Hojo, M., Meurer, J., Endo, T., Tasaka, M., and Shikanai, T. (2002) PGR5 is involved in cyclic electron flow around photosystem I and is essential for photoprotection in *Arabidopsis*. *Cell* **110,** 361–371 CrossRef Medline
10. DalCorso, G., Pesaresi, P., Masiero, S., Aseeva, E., Schünemann, D., Finazzi, G., Joliot, P., Barbato, R., and Leister, D. (2008) A complex containing PGRL1 and PGR5 is involved in the switch between linear and cyclic electron flow in *Arabidopsis*. *Cell* **132,** 273–285 CrossRef Medline
11. Hertle, A. P., Blunder, T., Wunder, T., Pesaresi, P., Pribil, M., Armbruster, U., and Leister, D. (2013) PGRL1 is the elusive ferredoxin-plastoquinone reductase in photosynthetic cyclic electron flow. *Mol. Cell* **49,** 511–523 CrossRef Medline
12. Nawrocki, W., Bailleul, B., Cardol, P., Rappaport, F., Wollman, F.-A., and Joliot, P. (2017) Cyclic electron flow in *Chlamydomonas reinhardtii*. *bioRxiv* CrossRef
13. Zhang, H., Whitelegge, J. P., and Cramer, W. A. (2001) Ferredoxin: $NADP^+$ oxidoreductase is a subunit of the chloroplast cytochrome $b_6f$ complex. *J. Biol. Chem.* **276,** 38159–38165 Medline
14. Okutani, S., Hanke, G. T., Satomi, Y., Takao, T., Kurisu, G., Suzuki, A., and Hase, T. (2005) Three maize leaf ferredoxin:NADPH oxidoreductases vary in subchloroplast location, expression, and interaction with ferredoxin. *Plant Physiol.* **139,** 1451–1459 CrossRef Medline
15. Joliot, P., and Johnson, G. N. (2011) Regulation of cyclic and linear electron flow in higher plants. *Proc. Natl. Acad. Sci. U.S.A.* **108,** 13317–13322 CrossRef Medline
16. Ilík, P., Pavlovič, A., Kouřil, R., Alboresi, A., Morosinotto, T., Allahverdiyeva, Y., Aro, E. M., Yamamoto, H., and Shikanai, T. (2017) Alternative electron transport mediated by flavodiiron proteins is operational in organisms from cyanobacteria up to gymnosperms. *New Phytol.* **214,** 967–972 CrossRef Medline
17. Chaux, F., Burlacot, A., Mekhalfi, M., Auroy, P., Blangy, S., Richaud, P., and Peltier, G. (2017) Flavodiiron proteins promote fast and transient $O_2$ photoreduction in *Chlamydomonas*. *Plant Physiol.* **174,** 1825–1836 CrossRef Medline
18. Takahashi, H., Clowez, S., Wollman, F. A., Vallon, O., and Rappaport, F. (2013) Cyclic electron flow is redox-controlled but independent of state transition. *Nat. Commun.* **4,** 1954 CrossRef Medline
19. Vallon, O., Bulte, L., Dainese, P., Olive, J., Bassi, R., and Wollman, F. A. (1991) Lateral redistribution of cytochrome $b_6/f$ complexes along thylakoid membranes upon state transitions. *Proc. Natl. Acad. Sci. U.S.A.* **88,** 8262–8266 CrossRef Medline
20. Fleischmann, M. M., Ravanel, S., Delosme, R., Olive, J., Zito, F., Wollman, F. A., and Rochaix, J. D. (1999) Isolation and characterization of photoautotrophic mutants of *Chlamydomonas reinhardtii* deficient in state transition. *J. Biol. Chem.* **274,** 30987–30994 CrossRef Medline
21. Iwai, M., Takizawa, K., Tokutsu, R., Okamuro, A., Takahashi, Y., and Minagawa, J. (2010) Isolation of the elusive supercomplex that drives cyclic electron flow in photosynthesis. *Nature* **464,** 1210–1213 CrossRef Medline
22. Terashima, M., Petroutsos, D., Hüdig, M., Tolstygina, I., Trompelt, K., Gäbelein, P., Fufezan, C., Kudla, J., Weinl, S., Finazzi, G., and Hippler, M. (2012) Calcium-dependent regulation of cyclic photosynthetic electron transfer by a CAS, ANR1, and PGRL1 complex. *Proc. Natl. Acad. Sci. U.S.A.* **109,** 17717–17722 CrossRef Medline
23. Takahashi, H., Schmollinger, S., Lee, J. H., Schroda, M., Rappaport, F., Wollman, F. A., and Vallon, O. (2016) PETO interacts with other effectors of cyclic electron flow in *Chlamydomonas*. *Mol. Plant* **9,** 558–568 CrossRef Medline
24. Terashima, M., Specht, M., Naumann, B., and Hippler, M. (2010) Characterizing the anaerobic response of *Chlamydomonas reinhardtii* by quantitative proteomics. *Mol. Cell. Proteomics* **9,** 1514–1532 CrossRef Medline
25. Hamel, P., Olive, J., Pierre, Y., Wollman, F. A., and de Vitry, C. (2000) A new subunit of cytochrome $b_6f$ complex undergoes reversible phosphorylation upon state transition. *J. Biol. Chem.* **275,** 17072–17079 CrossRef Medline
26. Lemaire, C., Girard-Bascou, J., Wollman, F.-A., and Bennoun, P. (1986) Studies on the cytochrome $b_6/f$ complex. I. Characterization of the complex subunits in *Chlamydomonas reinhardtii*. *Biochim. Biophys. Acta* **851,** 229–238 CrossRef
27. Stroebel, D., Choquet, Y., Popot, J. L., and Picot, D. (2003) An atypical haem in the cytochrome $b_6f$ complex. *Nature* **426,** 413–418 CrossRef Medline
28. Bergner, S. V., Scholz, M., Trompelt, K., Barth, J., Gäbelein, P., Steinbeck, J., Xue, H., Clowez, S., Fucile, G., Goldschmidt-Clermont, M., Fufezan, C., and Hippler, M. (2015) STATE TRANSITION7-dependent phosphorylation is modulated by changing environmental conditions, and its absence triggers remodeling of photosynthetic protein complexes. *Plant Physiol.* **168,** 615–634 CrossRef Medline
29. Pierre, Y., Breyton, C., Kramer, D., and Popot, J. L. (1995) Purification and characterization of the cytochrome $b_6f$ complex from *Chlamydomonas reinhardtii*. *J. Biol. Chem.* **270,** 29342–29349 CrossRef Medline
30. Seddon, A. M., Curnow, P., and Booth, P. J. (2004) Membrane proteins, lipids and detergents: not just a soap opera. *Biochim. Biophys. Acta* **1666,** 105–117 CrossRef Medline
31. Zoonens, M., and Popot, J. L. (2014) Amphipols for each season. *J. Membr. Biol.* **247,** 759–796 CrossRef Medline
32. Szyszka-Mroz, B., Pittock, P., Ivanov, A. G., Lajoie, G., and Hüner, N. P. (2015) The Antarctic psychrophile *Chlamydomonas* sp. UWO 241 preferentially phosphorylates a photosystem I-cytochrome $b_6/f$ supercomplex. *Plant Physiol.* **169,** 717–736 CrossRef Medline
33. Bulte, L., Gans, P., Rebeille, F., and Wollman, F. A. (1990) ATP control on state transitions *in vivo* in *Chlamydomonas reinhardtii*. *Biochim. Biophys. Acta* **1020,** 72–80 CrossRef
34. Chua, N. H., and Bennoun, P. (1975) Thylakoid membrane polypeptides of *Chlamydomonas reinhardtii*: wild-type and mutant strains deficient in photosystem II reaction center. *Proc. Natl. Acad. Sci. U.S.A.* **72,** 2175–2179 CrossRef Medline
35. Wollman, F.-A., and Lemaire, C. (1988) Studies on kinase-controlled state transitions in Photosystem II and $b_6f$ mutants from *Chlamydomonas reinhardtii* which lack quinone-binding proteins. *Biochim. Biophys. Acta* **933,** 85–94 CrossRef
36. Hankamer, B., Nield, J., Zheleva, D., Boekema, E., Jansson, S., and Barber, J. (1997) Isolation and biochemical characterisation of monomeric and dimeric photosystem II complexes from spinach and their relevance to the organisation of photosystem II *in vivo*. *Eur. J. Biochem.* **243,** 422–429 CrossRef Medline
37. Kurisu, G., Zhang, H., Smith, J. L., and Cramer, W. A. (2003) Structure of the cytochrome $b_6f$ complex of oxygenic photosynthesis: tuning the cavity. *Science* **302,** 1009–1014 CrossRef Medline

38. Choquet, Y., Zito, F., Wostrikoff, K., and Wollman, F. A. (2003) Cytochrome *f* translation in *Chlamydomonas* chloroplast is autoregulated by its carboxyl-terminal domain. *Plant Cell* **15,** 1443–1454 CrossRef Medline
39. Kuras, R., Saint-Marcoux, D., Wollman, F. A., and de Vitry, C. (2007) A specific *c*-type cytochrome maturation system is required for oxygenic photosynthesis. *Proc. Natl. Acad. Sci. U.S.A.* **104,** 9906–9910 CrossRef Medline
40. Yu, F., Li, N., and Yu, W. (2017) Exhaustively identifying cross-linked peptides with a linear computational complexity. *J. Proteome Res.* **16,** 3942–3952 CrossRef Medline
41. Källberg, M., Wang, H., Wang, S., Peng, J., Wang, Z., Lu, H., and Xu, J. (2012) Template-based protein structure modeling using the RaptorX web server. *Nat. Protoc.* **7,** 1511–1522 CrossRef Medline
42. Dumas, L., Zito, F., Blangy, S., Auroy, P., Johnson, X., Peltier, G., and Alric, J. (2017) A stromal region of cytochrome $b_6f$ subunit IV is involved in the activation of the Stt7 kinase in *Chlamydomonas*. *Proc. Natl. Acad. Sci. U.S.A.* **114,** 12063–12068 CrossRef Medline
43. Breyton, C., Chabaud, E., Chaudier, Y., Pucci, B., and Popot, J. L. (2004) Hemifluorinated surfactants: a non-dissociating environment for handling membrane proteins in aqueous solutions? *FEBS Lett.* **564,** 312–318 CrossRef Medline
44. Hovers, J., Potschies, M., Polidori, A., Pucci, B., Raynal, S., Bonneté, F., Serrano-Vega, M. J., Tate, C. G., Picot, D., Pierre, Y., Popot, J. L., Nehmé, R., Bidet, M., Mus-Veteau, I., Busskamp, H., *et al.* (2011) A class of mild surfactants that keep integral membrane proteins water-soluble for functional studies and crystallization. *Mol. Membr. Biol.* **28,** 171–181 CrossRef Medline
45. Tribet, C., Audebert, R., and Popot, J. L. (1996) Amphipols: polymers that keep membrane proteins soluble in aqueous solutions. *Proc. Natl. Acad. Sci. U.S.A.* **93,** 15047–15050 CrossRef Medline
46. Nagy, J. K., Kuhn Hoffmann, A., Keyes, M. H., Gray, D. N., Oxenoid, K., and Sanders, C. R. (2001) Use of amphipathic polymers to deliver a membrane protein to lipid bilayers. *FEBS Lett.* **501,** 115–120 CrossRef Medline
47. Picard, M., Dahmane, T., Garrigos, M., Gauron, C., Giusti, F., le Maire, M., Popot, J. L., and Champeil, P. (2006) Protective and inhibitory effects of various types of amphipols on the $Ca^{2+}$-ATPase from sarcoplasmic reticulum: a comparative study. *Biochemistry* **45,** 1861–1869 CrossRef Medline
48. Singh, S. K., Hasan, S. S., Zakharov, S. D., Naurin, S., Cohn, W., Ma, J., Whitelegge, J. P., and Cramer, W. A. (2016) Trans-membrane signaling in photosynthetic state transitions: redox- and structure-dependent interaction *in vitro* between STT7 kinase and the cytochrome $b_6f$ complex. *J. Biol. Chem.* **291,** 21740–21750 CrossRef Medline
49. Rochaix, J. D., Lemeille, S., Shapiguzov, A., Samol, I., Fucile, G., Willig, A., and Goldschmidt-Clermont, M. (2012) Protein kinases and phosphatases involved in the acclimation of the photosynthetic apparatus to a changing light environment. *Philos. Trans. R. Soc. Lond. B Biol. Sci.* **367,** 3466–3474 CrossRef Medline
50. Allen, J. F., Bennett, J., Steinback, K. E., and Arntzen, C. J. (1981) Chloroplast protein phosphorylation couples plastoquinone redox state to distribution of excitation energy between photosystems. *Nature* **291,** 25–29 CrossRef
51. Skinner, J. J., Wang, S., Lee, J., Ong, C., Sommese, R., Sivaramakrishnan, S., Koelmel, W., Hirschbeck, M., Schindelin, H., Kisker, C., Lorenz, K., Sosnick, T. R., and Rosner, M. R. (2017) Conserved salt-bridge competition triggered by phosphorylation regulates the protein interactome. *Proc. Natl. Acad. Sci. U.S.A.* **114,** 13453–13458 CrossRef Medline
52. Hemschemeier, A., and Happe, T. (2011) Alternative photosynthetic electron transport pathways during anaerobiosis in the green alga *Chlamydomonas reinhardtii*. *Biochim. Biophys. Acta* **1807,** 919–926 CrossRef Medline
53. Catalanotti, C., Yang, W., Posewitz, M. C., and Grossman, A. R. (2013) Fermentation metabolism and its evolution in algae. *Front. Plant Sci.* **4,** 150 Medline
54. Yamamoto, H., and Shikanai, T. (2013) In planta mutagenesis of Src homology 3 domain-like fold of NdhS, a ferredoxin-binding subunit of the chloroplast NADH dehydrogenase-like complex in *Arabidopsis*: a conserved Arg-193 plays a critical role in ferredoxin binding. *J. Biol. Chem.* **288,** 36328–36337 CrossRef Medline
55. Peden, E. A., Boehm, M., Mulder, D. W., Davis, R., Old, W. M., King, P. W., Ghirardi, M. L., and Dubini, A. (2013) Identification of global ferredoxin interaction networks in *Chlamydomonas reinhardtii*. *J. Biol. Chem.* **288,** 35192–35209 CrossRef Medline
56. Yang, W., Wittkopp, T. M., Li, X., Warakanont, J., Dubini, A., Catalanotti, C., Kim, R. G., Nowack, E. C., Mackinder, L. C., Aksoy, M., Page, M. D., D'Adamo, S., Saroussi, S., Heinnickel, M., Johnson, X., *et al.* (2015) Critical role of *Chlamydomonas reinhardtii* ferredoxin-5 in maintaining membrane structure and dark metabolism. *Proc. Natl. Acad. Sci. U.S.A.* **112,** 14978–14983 CrossRef Medline
57. Hanke, G. T., Okutani, S., Satomi, Y., Takao, T., Suzuki, A., and Hase, T. (2005) Multiple iso-proteins of FNR in *Arabidopsis*: evidence for different contributions to chloroplast function and nitrogen assimilation. *Plant Cell Environ.* **28,** 1146–1157 CrossRef
58. Mosebach, L., Heilmann, C., Mutoh, R., Gäbelein, P., Steinbeck, J., Happe, T., Ikegami, T., Hanke, G., Kurisu, G., and Hippler, M. (2017) Association of ferredoxin:$NADP^+$ oxidoreductase with the photosynthetic apparatus modulates electron transfer in *Chlamydomonas reinhardtii*. *Photosynth. Res.* **134,** 291–306 CrossRef Medline
59. Benz, J. P., Stengel, A., Lintala, M., Lee, Y. H., Weber, A., Philippar, K., Gügel, I. L., Kaieda, S., Ikegami, T., Mulo, P., Soll, J., and Bölter, B. (2009) *Arabidopsis* Tic62 and ferredoxin-NADP(H) oxidoreductase form light-regulated complexes that are integrated into the chloroplast redox poise. *Plant Cell* **21,** 3965–3983 CrossRef Medline
60. Jurić, S., Hazler-Pilepić, K., Tomasić, A., Lepedus, H., Jelicić, B., Puthiyaveetil, S., Bionda, T., Vojta, L., Allen, J. F., Schleiff, E., and Fulgosi, H. (2009) Tethering of ferredoxin:NADP plus oxidoreductase to thylakoid membranes is mediated by novel chloroplast protein TROL. *Plant J.* **60,** 783–794 CrossRef Medline
61. Yang, C., Hu, H., Ren, H., Kong, Y., Lin, H., Guo, J., Wang, L., He, Y., Ding, X., Grabsztunowicz, M., Mulo, P., Chen, T., Liu, Y., Wu, Z., Wu, Y., Mao, C., Wu, P., and Mo, X. (2016) LIGHT-INDUCED RICE1 regulates light-dependent attachment of LEAF-TYPE FERREDOXIN-$NADP^+$ OXIDOREDUCTASE to the thylakoid membrane in rice and *Arabidopsis*. *Plant Cell* **28,** 712–728 CrossRef Medline
62. Yadav, K. N., Semchonok, D. A., Nosek, L., Kouřil, R., Fucile, G., Boekema, E. J., and Eichacker, L. A. (2017) Supercomplexes of plant photosystem I with cytochrome b6f, light-harvesting complex II and NDH. *Biochim. Biophys. Acta Bioenerg.* **1858,** 12–20 CrossRef Medline
63. Tolleter, D., Ghysels, B., Alric, J., Petroutsos, D., Tolstygina, I., Krawietz, D., Happe, T., Auroy, P., Adriano, J. M., Beyly, A., Cuiné, S., Plet, J., Reiter, I. M., Genty, B., Cournac, L., *et al.* (2011) Control of hydrogen photoproduction by the proton gradient generated by cyclic electron flow in *Chlamydomonas reinhardtii*. *Plant Cell* **23,** 2619–2630 CrossRef Medline
64. Li, X., Zhang, R., Patena, W., Gang, S. S., Blum, S. R., Ivanova, N., Yue, R., Robertson, J. M., Lefebvre, P. A., Fitz-Gibbon, S. T., Grossman, A. R., and Jonikas, M. C. (2016) An indexed, mapped mutant library enables reverse genetics studies of biological processes in *Chlamydomonas reinhardtii*. *Plant Cell* **28,** 367–387 CrossRef Medline
65. Debuchy, R., Purton, S., and Rochaix, J. D. (1989) The argininosuccinate lyase gene of *Chlamydomonas reinhardtii*: an important tool for nuclear transformation and for correlating the genetic and molecular maps of the ARG7 locus. *EMBO J.* **8,** 2803–2809 CrossRef Medline
66. Rimbault, B., Esposito, D., Drapier, D., Choquet, Y., Stern, D., and Wollman, F. A. (2000) Identification of the initiation codon for the *atpB* gene in *Chlamydomonas* chloroplasts excludes translation of a precursor form of the $\beta$ subunit of the ATP synthase. *Mol. Gen. Genet.* **264,** 486–491 CrossRef Medline
67. Sturm, N. R., Kuras, R., Büschlen, S., Sakamoto, W., Kindle, K. L., Stern, D. B., and Wollman, F. A. (1994) The *petD* gene is transcribed by functionally redundant promoters in *Chlamydomonas reinhardtii* chloroplasts. *Mol. Cell. Biol.* **14,** 6171–6179 CrossRef Medline
68. Iwai, M., Takahashi, Y., and Minagawa, J. (2008) Molecular remodeling of photosystem II during state transitions in *Chlamydomonas reinhardtii*. *Plant Cell* **20,** 2177–2189 CrossRef Medline

69. Fischer, N., Sétif, P., and Rochaix, J. D. (1997) Targeted mutations in the *psaC* gene of *Chlamydomonas reinhardtii*: preferential reduction of $F_B$ at low temperature is not accompanied by altered electron flow from photosystem I to ferredoxin. *Biochemistry* **36,** 93–102 CrossRef Medline
70. Porra, R. J., Thompson, W. A., and Kriedemann, P. E. (1989) Determination of accurate extinction coefficients and simultaneous-equations for assaying chlorophyll-a and chlorophyll-b extracted with 4 different solvents: verification of the concentration of chlorophyll standards by atomic-absorption spectroscopy. *Biochim. Biophys. Acta* **975,** 384–394 CrossRef
71. Schägger, H., and von Jagow, G. (1987) Tricine-sodium dodecyl sulfate-polyacrylamide gel electrophoresis for the separation of proteins in the range from 1 to 100 kDa. *Anal. Biochem.* **166,** 368–379 CrossRef Medline
72. Wiśniewski, J. R., Zougman, A., Nagaraj, N., and Mann, M. (2009) Universal sample preparation method for proteome analysis. *Nat. Methods* **6,** 359–362 CrossRef Medline
73. Steinbeck, J., Ross, I. L., Rothnagel, R., Gäbelein, P., Schulze, S., Giles, N., Ali, R., Drysdale, R., Sierecki, E., Gambin, Y., Stahlberg, H., Takahashi, Y., Hippler, M., and Hankamer, B. (2018) Structure of a PSI-LHCI-cyt $b_6f$ supercomplex in *Chlamydomonas reinhardtii* promoting cyclic electron flow under anaerobic conditions. *Proc. Natl. Acad. Sci. U.S.A.* **115,** 10517–10522 CrossRef Medline